Available on CMS information server

CMS NOTE 2003/004

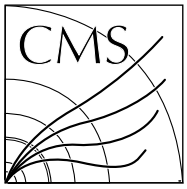

The Compact Muon Solenoid Experiment

CMS Note

Mailing address: CMS CERN, CH-1211 GENEVA 23, Switzerland

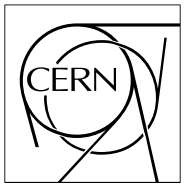

Trilepton+top signal from chargino-neutralino decays of MSSM charged Higgs bosons at the LHC

M. Bisset[a)]

Department of Physics, Tsinghua University, Beijing, P.R. China 100084

F. Moortgat[a)]

Department of Physics, University of Antwerpen, B-2610 Antwerpen, Belgium

S. Moretti[a,b)]

Department of Physics and Astronomy, University of Southampton, Highfield, Southampton SO17 1BJ, UK

Abstract

We perform for the Large Hadron Collider (LHC) a detailed study of charged Higgs boson production via the top-bottom quark associated mode followed by decays into a chargino and a neutralino, with masses and couplings as given by the general Minimal Supersymmetric Standard Model (MSSM). We focus our attention on the region of parameter space with $m_{H^\pm} > m_t$ and intermediate values of $\tan\beta$, where identification of $H^\pm$ via decays into Standard Model (SM) particles has proven to be ineffective. Modelling the CMS detector, we find that a signature consisting of three hard leptons accompanied by a hadronically reconstructed top quark plus substantial missing transverse energy, which may result from $H^\pm \to \widetilde{\chi}^\pm_{1,2}\widetilde{\chi}^0_{1,2,3,4}$ decays, can be made viable over a large variety of initially overwhelming SM and MSSM backgrounds, provided MSSM input parameters are favourable: notably, small $|\mu|$ and light sleptons are important prerequisites. We quantify these statements by performing a fairly extensive scan of the parameter space, including realistic hadron-level simulations, and delineate some potential discovery regions.

a) E-mails: bisset@mail.tsinghua.edu.cn, filip.moortgat@cern.ch, stefano.moretti@cern.ch.

b) Formerly at: Theory Division, CERN, CH-1211 Geneva 23, Switzerland and Institute for Particle Physics Phenomenology, University of Durham, Durham DH1 3LE, UK.

1 Introduction

A pair of spin-less charged Higgs bosons, $H^\pm$ (with mass $m_{H^\pm}$), arises in any Two-Higgs Doublet Model (2HDM) alongside a trio of neutral Higgs bosons — the CP-even 'light' h and 'heavy' H (*i.e.*, with $m_h < m_H$) scalars and the CP-odd pseudoscalar A (with mass m_A). Embedding a Type II 2HDM inside the attractive theoretical framework provided by Supersymmetry (SUSY) yields the MSSM (see [1]), wherein the particle content is limited to the known SM states (fermions and gauge bosons), their 'sparticle' counterparts (sfermions and gauginos) plus the five aforementioned Higgs bosons and their respective Higgsinos. Among the new massive sparticles predicted in the MSSM are the charginos and the neutralinos[1)], which are the mass eigenstate mixtures of the electroweak (EW) gauginos and the Higgsinos. Previous papers [2, 3] have demonstrated that $H^\pm$ decays into a chargino and a neutralino can probe regions of the MSSM parameter space where charged Higgs boson decays into SM particles and other Higgs bosons are swamped by backgrounds. In particular, $\tan\beta$ (the ratio of the vacuum expectation values of the up-type and down-type Higgs doublets) values between 3 and 10 were found to be in part accessible via $H^\pm \to \widetilde{\chi}_1^\pm \widetilde{\chi}_{2,3}^0$ decay modes (*i.e.*, charged Higgs boson decays into the lightest chargino and the second or third heaviest neutralino), when the final state includes three leptons (meaning electrons and/or muons)[2)].

Such $\tan\beta$ values fall in the so-called 'intermediate' regime wherein $H^\pm$ decays to SM objects (which may include neutral MSSM Higgs bosons) are undetectable at the LHC irrespective of the values chosen for other MSSM input parameters[3)]. This zone of undetectability, in part due to the $\sim (m_b^2 \tan\beta^2 + m_t^2/\tan\beta^2)$ coupling of the main $pp \to tH^-X$ + c.c. production mode, begins around $\tan\beta = 6$ or 7 for $m_{H^\pm} \sim m_t$ and spreads to encompass more and more $\tan\beta$ values (say, between 3 and 20) as $m_{H^\pm}$ grows larger. The rate suppression may be further exacerbated by the same $\tan\beta$ dependence in the $H^- \to b\bar{t}$ decays if there are other competing decay channels — naturally, if the $H^- \to b\bar{t}$ branching ratio (BR) is $\simeq 1$, it will remain so and there is no additional suppression of the bottom-top decay rate. The alternative MSSM decay channel $H^- \to hW^-$, which also yields $b\bar{b}W^-$ intermediate states (since $h \to b\bar{b}$), is only relevant within a minuscule $\tan\beta$ interval (roughly $\tan\beta \approx 2-3$) for $m_{H^\pm} \lesssim m_t$ — this lies close to the LEP2's excluded region. Then there is $H^- \to \tau\bar{\nu}_\tau$, which is limited to larger $\tan\beta$ values[4)], at best offering coverage down to $\tan\beta \sim 10$ for $m_{H^\pm} \sim m_t$ and contracting to even higher $\tan\beta$ values as $m_{H^\pm}$ grows larger [6]. (See references in [2, 3] for a list of phenomenological analyses of these SM decay modes of a charged Higgs boson.)

Considering such limitations, it is worthwhile pursuing further the $H^\pm \to$ inos decay modes initially probed in [2, 3][5)], expanding upon the results found therein and placing the analysis in a sounder phenomenological context. The improvements found herein go in three general directions. Firstly, the allowable parameter space is covered far more thoroughly, incorporating all possible chargino-neutralino decay modes into the analysis and including every conceivable path leading from a charged Higgs boson to a three leptons plus invisible energy final state. Secondly, investigation of the rôle of on- and off-shell sleptons (the SUSY partners of the leptons) is considerably deepened: as noted in the previous studies, if there is a light slepton, the leptonic BRs of the inos can be significantly enhanced (especially those of $\widetilde{\chi}_2^0$ and/or $\widetilde{\chi}_3^0$). Thirdly, signals are herein studied within a full event generator environment modelling the CMS detector and also includes an improved background analysis that encompasses potential MSSM background processes ([3] was a very preliminary account in both these respects while [2] only considered SM backgrounds and was carried out solely at the parton level).

The legacy of the CERN e^+e^- collider is a model independent limit on $m_{H^\pm}$ from charged Higgs pair production of order $M_{W^\pm}$ — 78.6 GeV is the current LEP2 bound [10]. Further, the current lower Higgs boson mass bound of approximately 114 GeV [10] can be converted within the MSSM into a minimal value for $m_{H^\pm}$ of ∼130–140 GeV, for $\tan\beta \simeq$ 3–4. This bound grows rapidly stronger as $\tan\beta$ is decreased while tapering very gradually as $\tan\beta$ is increased (staying in the 110–125 GeV interval for $\tan\beta \gtrsim 6$). For $m_{H^\pm} < m_t$, charged Higgs bosons could be discovered during Run 2 of the FNAL Tevatron [11], which has already begun taking data at $\sqrt{s}_{p\bar{p}} = 2$ TeV, by

---

1) We will refer to the charginos and neutralinos collectively as 'inos'.

2) The process is further identified by a hadronically reconstructed top quark from the tH^-X (or $\bar{t}H^+X$) production process, and via substantial missing transverse momentum from the lightest neutralinos, $\widetilde{\chi}_1^0$s, the stable Lightest Supersymmetric Particles (LSPs) which must eventually result from decays of the inos.

3) Not coincidentally, in roughly the same area coverage via the neutral Higgs sector is questionable [4, 5], particularly if the integrated luminosity is limited (say, ∼30 fb^{-1}). Further, the one neutral Higgs boson that may be detectable typically mimics a SM Higgs boson (this is the so-called 'decoupling scenario').

4) The $H^- \to s\bar{c}$ mode has a much reduced scope in comparison, because of the large QCD background.

5) Hadron collider signals from neutral MSSM Higgs boson decays into inos were studied in [5, 7], while MSSM Higgs bosons BRs to inos, emphasising invisible decays to a pair of LSPs, were presented in [8, 9].

exploiting their production in top and antitop quark decays ($t \to bH^+ + \text{c.c.}$) followed by $H^- \to \tau^- \bar{\nu}_\tau + \text{c.c.}$ [12]. In contrast, if $m_{H^\pm} \gtrsim m_t$ (our definition of a 'heavy' charged Higgs boson), one will necessarily have to wait until the advent of the LHC at CERN, with $\sqrt{s}_{pp} = 14\,\text{TeV}$, and thus this study will concentrate upon charged Higgs boson masses well above that of the top (anti)quark. This will also provide ample phase space to allow for decays into sparticles with masses above current experimental bounds.

There are also other processes where charged Higgs bosons (or A, to whose mass that of the $H^\pm$ is closely tied) enter as virtual particles at the one-loop level. These include neutral meson mixing ($K^0\bar{K}^0$, $D^0\bar{D}^0$ or $B^0\bar{B}^0$) and $Z \to b\bar{b}$ (R_b) [13], $b \to s\gamma$ decays [13, 14], $b \to c\tau\bar{\nu}_\tau$ decays [15] and the anomalous muon magnetic dipole moment [16]. The $b \to s\gamma$ decays are generally thought to be the most constraining [13] ($b \to c\tau\bar{\nu}_\tau$ becomes significant for very high values of $\tan\beta$). Here restrictions on $m_{H^\pm}$ are linked to a number of MSSM variables, notably including the masses of the lighter chargino and the stops. The $b \to s\gamma$ decays and the other higher order processes may well exclude some regions of the MSSM parameter space that are still allowed by the more direct limits from Higgs boson and sparticle searches at LEP2. However, definite bounds are quite difficult to delineate without restricting oneself to some subset of the allowed parameter space of the general MSSM by specifying a mechanism for how SUSY is to be broken. Studies which have delineated excluded regions resulting from these processes have invariably included additional assumptions about the behaviour of the theory at higher energy scales — such as in Minimal Supergravity (mSUGRA) for example, for which next-to-leading order (NLO) calculations have recently been performed [14]. There are also significant uncertainties in translating the experimental results into clear predictions about MSSM parameters [17]. Concerning limits from recent $(g-2)_\mu$ measurements, these are most restricting [16] when $\tan\beta$ is low ($\lesssim 3$) – a case which is not of particular interest for our process – and may be relaxed when smuons are light – a case which is of particular interest for our process.

2 MSSM Parameter Space

Analysing the usefulness of $H^\pm \to$ chargino-neutralino decays within the general MSSM parameter space is a fairly involved undertaking since many independent input parameters associated with just about all the (s)particle sectors of the model can play crucial rôles. From the Higgs sector we of course have $\tan\beta$ along with one input Higgs boson mass, taken herein as m_A, to which the tree-level masses of all the other Higgs bosons are pegged. These two inputs are largely sufficient for the SM decay modes, assuming sparticle decay modes are closed.

Squark masses, particularly stop masses, can drive significant radiative corrections to the tree-level Higgs boson masses, especially to m_h. In contrast, higher order corrections to the tree-level relation $m^2_{H^\pm} = m^2_A + M^2_{W^\pm}$ are typically quite small [18]. Thus the signal rate is insensitive to the choice of squark-sector inputs. Nevertheless, the coloured-sparticle sector affects the analysis in peripheral — but potentially crucial — ways. Firstly, the choice of the stop mass inputs can affect what regions of the MSSM parameter space are excluded via Higgstrahlung or the aforementioned $b \to s\gamma$ processes. The former would suggest choosing high stop inputs to help push m_h up above the LEP2 bounds, while the latter might prefer low stop inputs to cancel corrections due to a light chargino. Be such arguments as they may, there is considerable uncertainty in the resulting limits on the general MSSM parameter space, and these issues will not be addressed further. The second consideration is the size of squark and gluino backgrounds to our signature. Discussion of this will be postponed until the end of this section.

To specify the ino sector, the parameters M_2 and μ, in addition to $\tan\beta$, are required. M_1 is assumed to be determined from M_2 via gaugino unification (*i.e.*, $M_1 = \frac{5}{3}\tan^2\theta_W M_2$). This will determine the tree-level masses (to which the radiative corrections are quite modest) of the inos along with their couplings to the Higgs bosons. However, this is not enough, for the inos (except for $\widetilde{\chi}^0_1$) must also decay – preferably into leptons for easy detection. To calculate the leptonic ino BRs, one must designate the properties of the slepton sector, since light sleptons can greatly enhance said BRs [2, 3, 19]. Inputs (assumed to be flavour-diagonal) from the slepton sector are the left and right soft slepton masses for each of the three generations (selectrons, smuons, and staus) and the trilinear 'A-terms' which come attached to Yukawa factors and thus only A_τ has a potential impact. *A priori*, all six left and right mass inputs (and A_τ) are independent. However, in most models currently advocated, one has $m_{\tilde{e}_R} \simeq m_{\tilde{\mu}_R}$ and $m_{\tilde{e}_L} \simeq m_{\tilde{\mu}_L}$. We will assume such equalities to hold.

To maximise leptonic ino BR enhancement, sleptons should be made as light as possible. But direct searches at LEP2 [20] place significant limits on slepton masses: $m_{\tilde{e}_1} \geq 99.0\,\text{GeV}$, $m_{\tilde{\mu}_1} \geq 91.0\,\text{GeV}$, $m_{\tilde{\tau}_1} \geq 85.0\,\text{GeV}$ (these assume that the slepton is not nearly-degenerate with the LSP) and $m_{\tilde{\nu}} \geq 43.7\,\text{GeV}$ (from studies at the Z pole). Furthermore, the sneutrino masses are closely tied to the left soft mass inputs, and, to avoid extra controversial assumptions, we will restrict ourselves to regions of the MSSM parameter space where the LSP is the lightest neutralino rather than a sneutrino. To optimise the ino leptonic BRs without running afoul of the LEP2 limits,

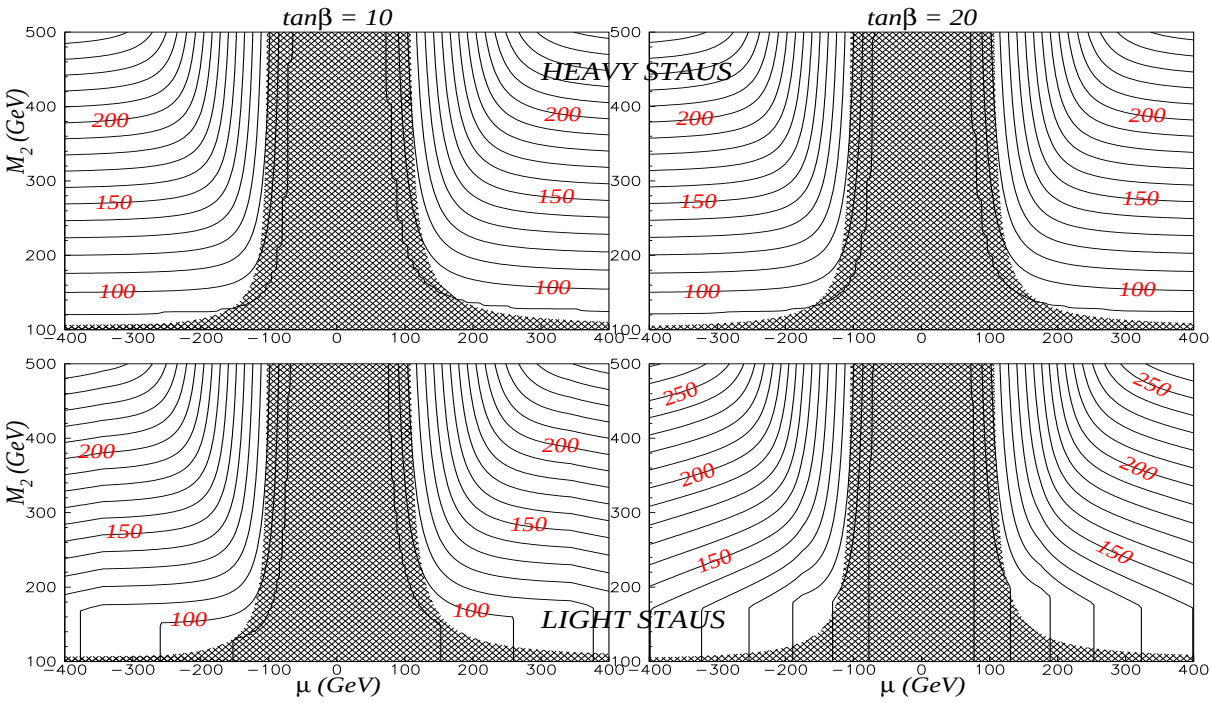

Figure 1: Minimum allowed soft slepton mass, given constraints as described in the text. In the upper (lower) two plots, soft stau mass inputs are set 100 GeV above (degenerate with) those of the first two generations. $A_\ell = 0$ in all cases. The shaded areas are excluded by LEP.

it is best to set $m_{\tilde{\ell}_R} = m_{\tilde{\ell}_L}$. If all three generations have the same soft inputs (with $A_\tau = 0$), then the slepton sector is effectively reduced to one optimal input value (which we identify with $m_{\tilde{\ell}_R}$). However, since ino decays to tau-leptons are generally not anywhere near as beneficial as are ino decays to electrons or muons, it would be even better if the stau inputs were significantly above those of the first two generations. This would enhance the inos' BRs into electrons and muons. In the general MSSM, we are of course free to choose the inputs as such. Doing so would also weaken restrictions from LEP2, especially for high $\tan\beta$ values. If we set the soft stau mass inputs 100 GeV above those of the other sleptons (with A_τ still kept at zero), the lowest allowable slepton masses, presented in the M_2 *vs.* μ plane for $\tan\beta = 10$ and 20, are as shown in the upper pair of plots in Fig. 1, while if all three generations have the same soft inputs we obtain the lower pair of plots in Fig. 1.

Incorporating such optimal slepton inputs and then scanning over the ino parameters M_2 and μ, for a couple of values of $\tan\beta$ and m_A, yields Fig. 2 for BR$(H^\pm \to 3\ell N)$, where ℓ may be either $e^\pm$ or $\mu^\pm$ and N represents any number of undetectable final state particles (either LSPs and/or neutrinos). In these plots, and in plots to be shown hereafter, all possible charged Higgs boson decay modes which can result in a final state with three charged leptons and no hadronic activity are included, except for leptons coming from tau decays. In this figure, including ℓs from decaying taus would not noticeably affect the BRs since the staus which could greatly enhance tau production are pushed up in mass.

As expected, BRs are larger for the $m_A = 500$ GeV plots on the right than for the $m_A = 300$ GeV plots on the left since more 3ℓ-producing $H^\pm \to$ inos decay modes open up as $m_{H^\pm}$ increases. BRs also decline as $\tan\beta$ is raised from 10 to 20. If instead the three slepton generations have degenerate soft mass inputs, then Fig. 3 is obtained. Here m_A is fixed at 500 GeV and the left- and right-hand plots depict, respectively, BRs without and with the inclusion of ℓs from tau decays. Overall rates drop relative to those in Fig. 2 since: (i) the slepton mass inputs must be set higher to evade LEP2 constraints; and (ii) charged Higgs boson decays leading to staus via inos – which are now very significant – often result in hadronic final states rather than purely leptonic ones.

Note from Figs. 2 & 3 that low values for $|\mu|$ are strongly favoured. This can be understood by inspecting the

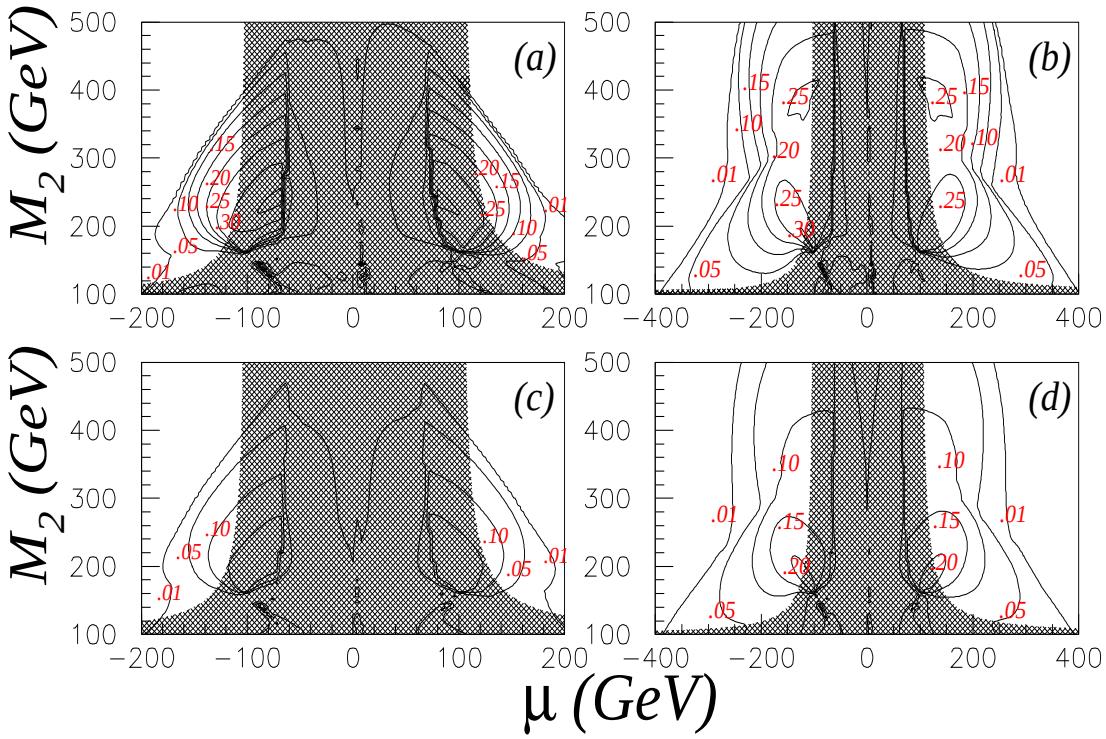

Figure 2: BR($H^\pm \to 3\ell N$), where $\ell = e^\pm$ or $\mu^\pm$ and N represents invisible final state particles, with $(m_A, \tan\beta) =$ (a) (300 GeV, 10), (b) (500 GeV, 10), (c) (300 GeV, 20), (d) (500 GeV, 20). Slepton mass inputs are optimised as in the upper plots of Fig. 1. The shaded areas are excluded by LEP.

tree-level decay width formula for $H^\pm \to \widetilde{\chi}_i^\pm \widetilde{\chi}_j^0$ [9],

$$\Gamma(H^\pm \to \widetilde{\chi}_i^\pm \widetilde{\chi}_j^0) = \frac{g^2\lambda^{1/2}[(F_L^2+F_R^2)(m_{H^\pm}^2 - m_{\widetilde{\chi}_i^\pm}^2 - m_{\widetilde{\chi}_j^0}^2) - 4\epsilon F_L F_R m_{\widetilde{\chi}_i^\pm} m_{\widetilde{\chi}_j^0}]}{16\pi m_{H^\pm}^3}, \tag{1}$$

$$\begin{aligned} F_L &= \cos\beta[N_{j4}V_{i1} + \sqrt{\tfrac{1}{2}}(N_{j2} + N_{j1}\tan\theta_W)V_{i2}], \\ F_R &= \sin\beta[N_{j3}U_{i1} - \sqrt{\tfrac{1}{2}}(N_{j2} + N_{j1}\tan\theta_W)U_{i2}], \end{aligned} \tag{2}$$

where ϵ is the sign convention for the neutralino mass eigenstates, g is the $SU(2)_L$ coupling and $\lambda = (m_{H^\pm}^2 - m_{\widetilde{\chi}_i^\pm}^2 - m_{\widetilde{\chi}_j^0}^2)^2 - 4m_{\widetilde{\chi}_i^\pm}^2 m_{\widetilde{\chi}_j^0}^2$. V_{i1} & U_{i1} (V_{i2} & U_{i2}) give the gaugino (Higgsino) component of chargino $\widetilde{\chi}_i^\pm$ while N_{j1} & N_{j2} (N_{j3} & N_{j4}) give the gaugino (Higgsino) components of neutralino $\widetilde{\chi}_j^0$. We immediately see from F_L and F_R that if the chargino and the neutralino are both pure gauginos (the SUSY counterparts of charged Higgs bosons decay into two gauge bosons — for which there is no coupling at tree level) or both pure Higgsinos, then the tree-level decay width is zero. Simple phase space considerations favouring decays to lighter inos then disfavour situations in which $|\mu| \gg M_2$ (or $|\mu| \ll M_2$) in which case light charginos *and* light neutralinos are almost pure gauginos (Higgsinos) — $|\mu| \sim M_2$ is preferred, ideally with both values as small as possible to make the lighter inos as light as possible (to the extent that LEP2 constraints permit). Thus the optimal region for high $H^\pm \to$ inos BRs is where inos are mixtures of gauginos and Higgsinos just above the bends of the LEP2 parameter space bounds (shaded regions in Figs. 1–3) in the M_2 *vs.* μ plane[6].

[6] For higher values of $\tan\beta$, $F_L \propto \cos\beta$ is small compared to $F_R \propto \sin\beta$. So the $H^\pm$ to $SU(2)_L$-wino Higgsino decay SUSY-related to $H^\pm \to W^\pm h$ (where h is now mostly from the down-coupling Higgs doublet and so the corresponding Higgsino has a dominating N_{j4} component entering into F_L) is also small. But the actual inos may not have such compositions. Furthermore, the signature of $H^\pm \to$ inos is more distinctive than that of $H^\pm \to hW^\pm$ — even if the BRs for the two processes were similar, more events from the former than from the latter would remain after sufficient cuts were made to eliminate backgrounds.

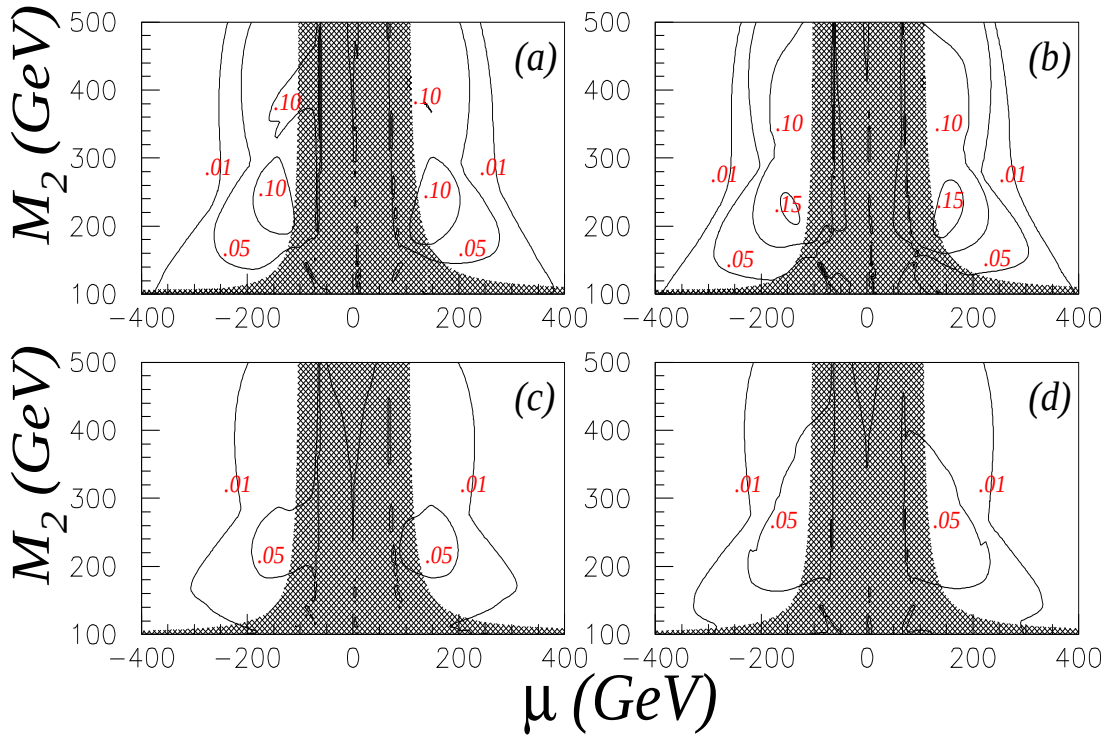

Figure 3: BR($H^\pm \to 3\ell N$), where $\ell = e^\pm$ or $\mu^\pm$ and N represents invisible final state particles; ℓs resulting from tau decays (are not) are included for plots on the (left-) right-hand side; $m_A = 500\,\text{GeV}$ and $\tan\beta = 10$ in plots (a) and (b), 20 in plots (c) and (d). Slepton mass inputs for all three generations are optimised as in the lower plots of Fig. 1. The shaded areas are excluded by LEP.

In addition, one would like to optimise $H^\pm \to \widetilde{\chi}_i^\pm \widetilde{\chi}_j^0$ decays where $j \neq 1$ to obtain the vast majority of the decays generating three leptons. Since $M_1 \simeq \frac{1}{2}M_2$, $M_2 \lesssim |\mu|$ generates an LSP that is mostly a $U(1)_Y$ bino and a somewhat gaugino-dominated chargino — which is bad for BR($H^\pm \to \widetilde{\chi}_1^\pm \widetilde{\chi}_1^0$) — but also makes for a quite light LSP, which over-compensates for the sub-optimal coupling. To increase the other $H^\pm \to$ light inos BRs, the mass of the LSP may be raised by making M_2 somewhat larger than $|\mu|$. Thus the final perscription for optimal rates is for small $|\mu|$ values and slightly larger, but still small to moderate values for M_2.

The charged Higgs boson BRs must now be tied to the production rate to obtain an expected number of signal events. Lowest order (LO) results from the parton-level process $gb \to tH^-$ are strongly dependent on which b-quark Parton Distribution Function (PDF) is chosen for convolution and on the scale at which α_s is evaluated. Moreover, the b-quark in the initial state originates with a gluon splitting into a $b\bar{b}$ pair inside the proton, so that the above $2 \to 2$ process (when convoluted with initial state radiation involving $g \to b\bar{b}$ in the backward evolution) can alternatively be taken as the $2 \to 3$ hard scattering subprocess $gg \to \bar{b}tH^-$ interfaced to gluon PDFs. The two descriptions have complementary strengths: the former most aptly describes 'inclusive' tH^-X final states, as it re-sums to all orders large terms of the form $\alpha_s \log(Q/m_b)$ (typically $Q \simeq m_t + M_{H^\pm}$), which are absorbed in the phenomenological PDF of the initial b-quark, while the latter modelling is better at describing 'exclusive' observables, as it accounts for the correct kinematic behaviour at large transverse momentum of the additional (or spectator) b-quark in the final state. Yet contributions from the two processes cannot simply be summed. In fact, the first term of the b-quark PDF is given by the perturbative solution to the DGLAP equation

$$b'(x,Q) = \frac{\alpha_S}{\pi} \log\left(\frac{Q}{m_b}\right) \int_x^1 \frac{dy}{y} P_{gb}\left(\frac{x}{y}\right) g(y,Q), \tag{3}$$

where $P_{gb}(z) = (z^2 + (1-z)^2)/2$ is the gluon-to-b splitting function, and the resulting contribution to $gb \to tH^-$ is already accounted for by $gg \to \bar{b}tH^-$ in the collinear limit. Thus, when combining the $2 \to 2$ and $2 \to 3$ processes, the above contribution should be subtracted from the former to avoid double counting [21]. An alternative approach [22] involves specifying a threshold in the transverse momentum of the spectator b-quark, $p_T^{b-\text{thr}}$, and then utilising

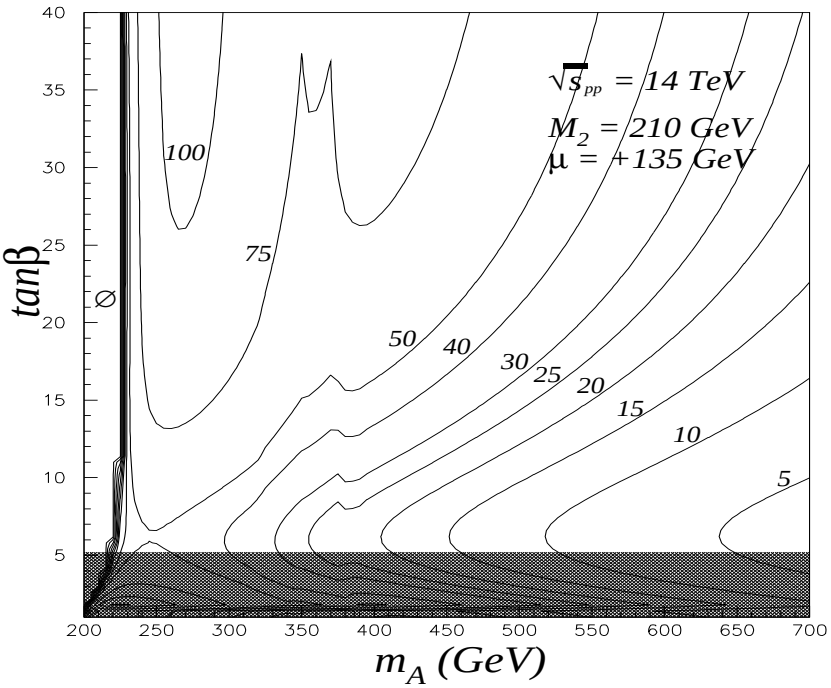

Figure 4: $\sigma(pp \to tH^- X \ + \ \text{c.c.}) \times \text{BR}(H^\pm \to 3\ell N)$ (in fb), where $\ell = e^\pm$ or $\mu^\pm$ and N represents invisible final state particles: M_2 and μ are as noted, and ℓs from tau decays are included. Slepton mass inputs are optimised as in the upper plots of Fig. 1. The LEP2 $M_{\widetilde{\chi}_1^\pm}$ limit excludes the shaded region, and the $\emptyset$ on the left signifies where the BR is virtually zero.

$2 \to 2$ kinematics when $p_T^b < p_T^{b-\text{thr}}$ and $2 \to 3$ kinematics for $p_T^b > p_T^{b-\text{thr}}$. This is particularly well-suited to Monte Carlo (MC) event simulations since it does not involve making the aforementioned subtraction with its associated negative weights. Both techniques yield cross section values midway between the larger predictions from $gb \to tH^-$ and the smaller ones from $gg \to \bar{b}tH^-$ (the latter being as much as a factor of 3–4 below the former).

Both approaches are less sensitive to the choice of the b-quark PDF and the factorisation scale, Q, than if the two processes were considered separately. However, in each case, only some parts of the NLO corrections are accounted for, finally yielding a negative NLO contribution. Quite importantly, recent results [23] have proved that full NLO corrections to the $2 \to 2$ process (*i.e.*, including both one-loop and radiative QCD corrections) yield an overall K-factor much larger than one, overturning the negative corrections obtained via the above procedures. Thus it is no longer justifiable to adopt normalisations based on these techniques.

Since most of the backgrounds are only known to LO accuracy, we used the MSSM implementation [24] of the HERWIG [25] event generator to simulate the $gb \to tH^-$ process and the various backgrounds using the default LO PDFs and α_s, without any additional K-factors. This partly explains the improvement to be seen herein relative to Ref. [3], where normalisation was via the old subtraction procedure. Nonetheless, we still regard our results as conservative since the dominant backgrounds (after cuts) are $t\bar{t}$ production, which has a similar QCD K-factor to that of the signal, and irreducible contributions from direct neutralino-chargino pair production, which, being EW processes at tree level, have smaller QCD corrections (of the order of 20% or so [26]). Yet one should also verify that the additional b-quark at high transverse momentum produced by the $gg \to \bar{b}tH^-$ contribution, which is not present in the (infrared dominated) backward evolution of the $2 \to 2$ process' initial b-quark, does not render untrustworthy a kinematical analysis done solely utilising the $2 \to 2$ process. We have confirmed this by also running HERWIG with $gg \to \bar{b}tH^-$ as the hard subprocess, adopting our usual selection cuts, and checking that in fact observable quantities (distributions and event rates) are not significantly affected by the presence of a spectator b-quark in the detector. All results shown will correspond to the outputs of the $2 \to 2$ process.

Fig. 4 shows $\sigma(pp \to tH^- X \ + \ \text{c.c.})$ with the subsequent decay $H^\pm \to 3\ell N$, where M_2 and μ are fixed at the favourable values of 210 GeV and 135 GeV, respectively — leading to the exclusion of $\tan\beta$ values below ~ 5 by the 103 GeV LEP2 lower bound on the chargino mass [20][7]. In the plot, the preference for high and low values

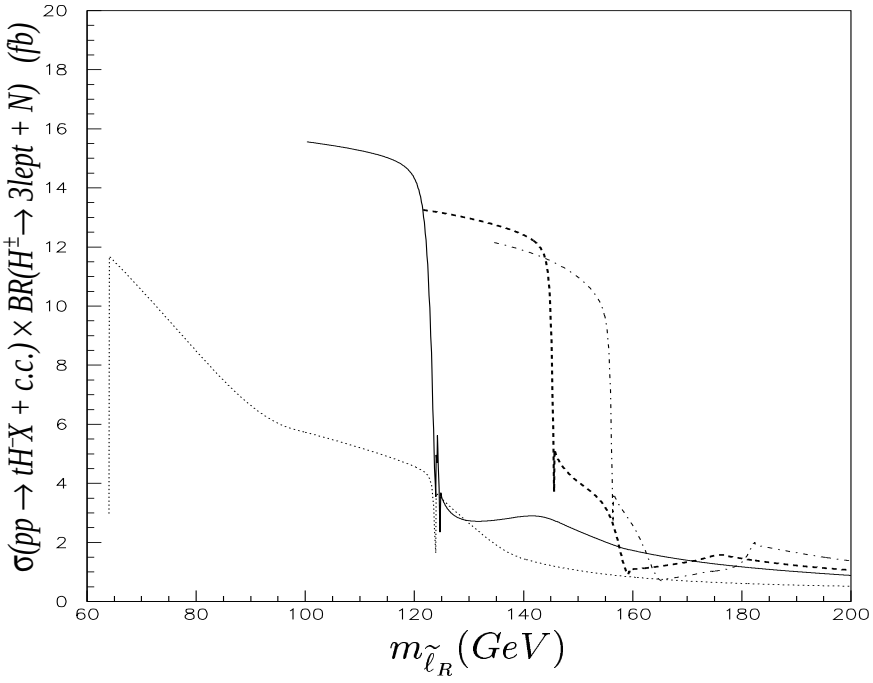

Figure 5: $\sigma(pp \to tH^- X + \text{c.c.}) \times \text{BR}(H^\pm \to 3\ell N)$ (in fb), where $\ell = e^\pm$ or $\mu^\pm$ and N represents invisible final state particles, *vs.* $m_{\tilde{\ell}_R}$, the soft slepton mass input for the first two generations (soft stau mass inputs are pushed up by an additional 100 GeV, $A_\tau = 0$). The set (M_2, μ) is fixed at $(210\,\text{GeV}, +135\,\text{GeV})$ for Parameter Set A (solid curve), at $(280\,\text{GeV}, +150\,\text{GeV})$ for Parameter Set B (thick dashed curve) and at $(300\,\text{GeV}, -150\,\text{GeV})$ for Parameter Set C (dot-dashed curve). The dotted curve replaces $m_{\tilde{\ell}_L} = m_{\tilde{\ell}_R}$ in Parameter Set A with $m_{\tilde{\ell}_L} = m_{\tilde{\ell}_R} + 100\,\text{GeV}$. The curves are terminated at the left where they would be LEP2 excluded, including the additional condition that $m_{\tilde{\nu}} > m_{\widetilde{\chi}_1^0}$; ℓs from tau decays are included.

of $\tan\beta$ so well-known for the raw $pp \to tH^- X$ cross section remains, though rates are nevertheless sufficient to seek a visible signal even in the intermediate $\tan\beta$ region via our characteristic signature.

It is instructive to next isolate the dependence of the signal rate upon the masses of the sleptons[8]. This is done in Fig. 5 for three choices of the other relevant MSSM parameters. All combinations fix $\tan\beta$ at 10 and m_A at 500 GeV. Parameter Set A (solid curve in Fig. 5) also sets $\mu = 135\,\text{GeV}$ and $M_2 = 210\,\text{GeV}$ (as in Fig. 4), while Parameter Set B (thick dashed curve in Fig. 5) has $\mu = 150\,\text{GeV}$ and $M_2 = 280\,\text{GeV}$ and Parameter Set C (dot-dashed curve in Fig. 5) adopts $\mu = -150\,\text{GeV}$ and $M_2 = 300\,\text{GeV}$ (these same parameter sets will also be used in the forthcoming detector simulation analysis). The horizontal axis in Fig. 5 is the *soft* slepton mass input (as before, left and right soft masses are degenerate and A-terms are zero). Bear in mind that this is not the same as the physical masses of the various sleptons, which also have so-called D-term contributions. The curves are terminated on the left side at the point where LEP experiments preclude the resulting light sleptons. Also shown by the dotted curve is the effect of removing the equality $m_{\tilde{\ell}_L} = m_{\tilde{\ell}_R}$: in this case $m_{\tilde{\ell}_L} = m_{\tilde{\ell}_R} + 100$ GeV while all the other MSSM parameters are the same as in Parameter Set A.

Focusing the account upon the two curves relating to Parameter Set A (features of the other curves are seen to be qualitatively similar), a sharp drop is seen around $m_{\tilde{\ell}_R} \sim 123 - 125\,\text{GeV}$ where the second neutralino becomes degenerate with the charged selectrons and smuons and also where the lighter chargino becomes degenerate with the sneutrinos (of the first two generations). The drop is due to the closing of the two-body decay modes $\widetilde{\chi}_2^0 \to \tilde{\ell}^\pm \ell^\mp$ and $\widetilde{\chi}_1^+ \to \tilde{\nu}_\ell \ell^+$, where $\tilde{\ell}^\pm$ and $\tilde{\nu}_\ell$ are on-mass-shell. Although the two-body decay modes close at this point, the sleptons still make their presence felt in the associated three-body decay modes via off-shell contributions. A

[7] For this choice of input parameters, the $m_{\widetilde{\chi}_1^\pm}$ bound is *probably* more restrictive than the one from Higgstrahlung, $e^+e^- \to hZ$ (and hA); however, this will not be true for other choices of M_2 and μ, such as those considered in the next paragraph. Note that the location of the Higgstrahlung bound is quite vague due to uncertainties in the radiatively-corrected mass m_h and errors in the measured value of m_t.

[8] Though sleptons are light, direct $H^\pm$ BRs to slepton pairs are at the sub-percent level. Sleptons meaningfully influence charged Higgs boson leptonic BRs via the sleptons' involvement in subsequent ino decays.

modest rise in the rate occurs for the solid curve as $m_{\tilde{\ell}_R}$ reaches $\sim$146 GeV where the second neutralino and the sneutrinos (of the first two generations) become degenerate and the 'spoiler' modes, $\widetilde{\chi}_2^0 \to \tilde{\nu}_\ell \nu_\ell$ — which result in no charged leptons — become inaccessible, consequently allowing BRs for the ℓ-producing channels to rise. This feature is absent for the dotted curve, with $m_{\tilde{\ell}_L} = m_{\tilde{\ell}_R} + 100$ GeV, since two-body ino decay modes to the now too heavy sneutrinos are not open. Yet despite the absence of the spoiler modes, rates remain lower in this case because $\tilde{\ell}_L$s are also heavy, simultaneously weakening the rate to charged leptons (when both are accessible and neither is phase-space suppressed, ino decays to either $\tilde{\ell}_L$s or to $\tilde{\nu}_\ell$s may be larger, depending on the composition of the neutralino). Note also that the dip at $m_{\tilde{\ell}_R} \sim 123 - 125$ GeV is less pronounced since now only two-body decay modes to $\tilde{\ell}_R$s are turning off at this point rather than to both left and right charged sleptons as in the solid curve. Lower values of $m_{\tilde{\ell}_R}$ are now possible since our (perhaps unnecessarily restrictive) requirement that $m_{\tilde{\nu}} > m_{\widetilde{\chi}_1^0}$ is satisfied for lower $m_{\tilde{\ell}_R}$ values. However, even going to such modest $m_{\tilde{\ell}_R}$ values does not compensate for the enhancement obtained when $m_{\tilde{\ell}_L} = m_{\tilde{\ell}_R}$ and the two-body modes to left charged sleptons are available. Thus the peak magnitude is appreciably lower for the dotted curve (confirming that $m_{\tilde{\ell}_L} = m_{\tilde{\ell}_R}$ is the optimal setup)[9].

For Parameter Set A, with $m_{\tilde{\ell}_R}$ set to 110 GeV, the largest contributor to the signal events is in fact[10] $H^\pm \to \widetilde{\chi}_1^\pm \widetilde{\chi}_2^0$ (35.2%), followed closely by $H^\pm \to \widetilde{\chi}_2^\pm \widetilde{\chi}_2^0$ (34.8%) and then $H^\pm \to \widetilde{\chi}_1^\pm \widetilde{\chi}_4^0$ (19.3%), $H^\pm \to \widetilde{\chi}_2^\pm \widetilde{\chi}_3^0$ (6.5%), and small contributions from $H^\pm \to \widetilde{\chi}_1^\pm \widetilde{\chi}_3^0$ (3.0%) and $H^\pm \to \widetilde{\chi}_2^\pm \widetilde{\chi}_1^0$ (1.2%) (here, the three ℓs all come from the $\widetilde{\chi}_2^\pm$); $H^\pm \to \widetilde{\chi}_1^\pm \widetilde{\chi}_{2,3}^0$ channels do not lead to most of the prospective signal events, contrary to what was assumed in Ref. [2]. Nevertheless, rates seen in Fig. 5 are still closely linked to $m_{\widetilde{\chi}_1^\pm}$ and $m_{\widetilde{\chi}_2^0}$ since $\widetilde{\chi}_1^\pm$ and/or $\widetilde{\chi}_2^0$ are present in most (92.3% for Set A) events, and, even if one (or both) is not in the ino pair to which $H^\pm$ directly decays, the heavier inos into which $H^\pm$ does decay in turn sometimes decay into these lighter inos (and charged leptons or neutrinos) to generate the signal events. With so many contributing channels, some of which involve multiple sparticle to sparticle decay chains, simulation of the signal with a robust event generator is imperative to ascertain the percentage of the events predicted utilising sparticle BR assignments that survive the cuts needed to sufficiently identify the signature and eliminate the backgrounds.

Returning now to the question of potential backgrounds from coloured-sparticle production processes, gluinos and squarks of the first two generations *may* in principle produce multi-lepton events with top quarks; however, in practice, top quarks are quite often not present in such events. Further, the limit on the squark (gluino) masses from Tevatron studies is now at least $\sim$260 GeV ($\sim$190 GeV) [27], and will rise if Tevatron searches continue to be unsuccessful. In addition, if the gaugino unification assumption also encompasses the gluino, then the gluino mass would be in the range $\sim$700–1000 GeV for the points being considered, and (at least in mSUGRA-inspired scenarios) squarks are expected to have heavier or at least comparable masses [28]. Thus there is substantial rationale for limiting this analysis to heavy gluino and squarks (of the first two generations) masses.

Stops are different though. Stringent experimental limits from LEP2 on stop masses only set a lower bound of $\sim$100 GeV [20], and stop pair production will generally lead to events containing top quarks. Possible decay chains that could mimic our signal events include for example $\widetilde{t}\widetilde{t}^* \to \widetilde{\chi}_1^0(t \to b\ell\nu) + (\widetilde{\chi}_2^0 \to \widetilde{\chi}_1^0 \ell\ell)(t \to \text{hadrons})$ and $\widetilde{t}\widetilde{t}^* \to (\widetilde{\chi}_1^+ \to \widetilde{\chi}_1^0 \ell\nu)b + (\widetilde{\chi}_2^0 \to \widetilde{\chi}_1^0 \ell\ell)(t \to \text{hadrons})$. Note though that such processes do have an extra b-jet (typically with high p_T) beyond that expected from $gb \to (t \to \text{hadrons})\ (H^- \to \widetilde{\chi}_i^- \widetilde{\chi}_j^0 \to 3\ell N)$ where N may be any number of colourless neutral stable particles. Fortunately, our studies indicate that the extra b-jet that is present in the $2 \to 3$ charged Higgs boson production process tends to be rather soft. So a cut on extra hard jets in the event does tend to remove the background from stop pair production (as well as that from squark and gluino production in general).

In keeping with the optimal strategy outlined above for the slepton sector, stops are made heavy to minimise this potential background. Thus we deal only with the MSSM backgrounds that must be present: that from direct ino pair production (since we require $H^\pm \to$ inos, the inos must be relatively light), and what coloured-sparticle backgrounds still remain when we have heavy gluinos and *all* squark inputs pushed up to 1 TeV. A more in depth study of light stops possibly mimicking our signal will be presented in an upcoming analysis [29].

3 mSUGRA Parameter Space

Before initiating the detector simulation analysis, we would like to document the potential for utilising the '$3\ell + t$' signature from $H^\pm \to$ inos in the more restrictive mSUGRA parameter space. As we will soon see, here prospects

[9] Setting $m_{\tilde{\ell}_R} > m_{\tilde{\ell}_L}$ shifts the curve to the right and slightly lowers the peak plateau.

[10] Numbers include leptons from decaying taus, but said inclusion only causes slight changes.

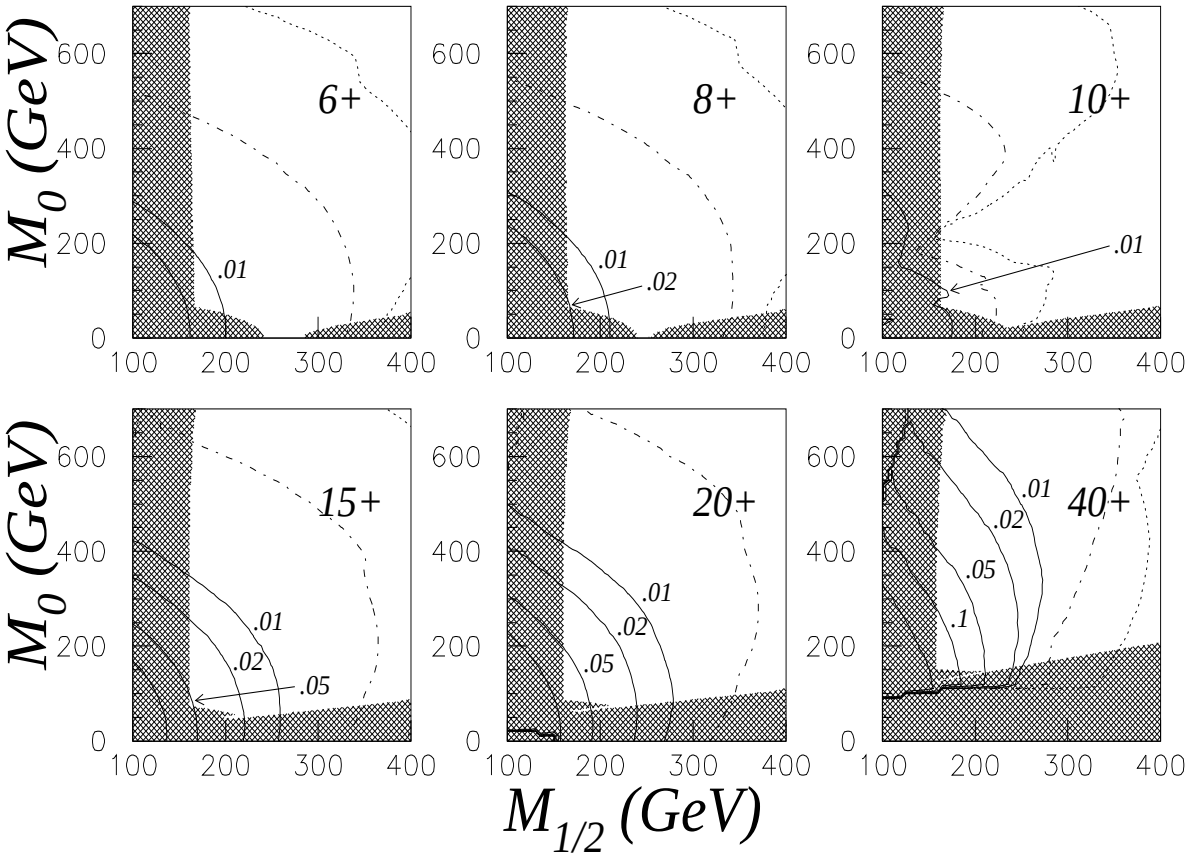

Figure 6: $\sigma(pp \to tH^- X \ + \ \text{c.c.})$ (in fb) multiplied by BR$(H^\pm \to 3\ell N)$, where $\ell = e^\pm$ or $\mu^\pm$ and N represents invisible final state particles, for a spread of mSUGRA parameter sets in the M_0 *vs.* $M_{\frac{1}{2}}$ plane; $A_0 = 0$ in all plots and ℓs resulting from tau decays are included. The number in the upper right of each plot is the $\tan\beta$ value followed by the sign of μ. The dot-dashed (dotted) contours are for 10^{-3} fb (10^{-4} fb). Solid contours for $\sigma\times$BR ≥ 0.01 fb have values as marked on the plots. The shaded regions are excluded by theoretical considerations or LEP2 measurements (save that constraints from Higgstrahlung are not applied).

are quite bleak. In mSUGRA, the free parameters are generally set as $\tan\beta$, a universal gaugino mass defined at the Grand Unification Theory (GUT) scale ($M_{\frac{1}{2}}$), a universal GUT-level scalar mass (M_0), a universal GUT-level trilinear scalar mass term (A_0), and the sign of μ. As already noted, the signal has a strong preference for low values of $|\mu|$. Yet in the mSUGRA scenario, $|\mu|$ is not a free parameter — it is closely tied to the masses of the scalar Higgs bosons via the M_0 input. Furthermore, the different soft slepton mass inputs can no longer be set independently: in particular, when evolved down to the EW scale using renormalisation group equations, the staus' soft inputs tend to be lower than those of sleptons from the first two generations rather than higher as was put in by hand in the more favourable MSSM parameter set choices of the preceding section. Fig. 6 shows the values for $\sigma(pp \to tH^- X \ + \ \text{c.c.}) \times \text{BR}(H^\pm \to 3\ell N)$ obtained for several discrete values of $\tan\beta$ and $\mu > 0$ (analogous plots for $\mu < 0$ are similar) with A_0 set to zero. The excluded regions shown take into account constraints from LEP2 save that coming from Higgstrahlung[11)], but not additional constraints[12)] from $b \to s\gamma$, $g_\mu - 2$ and other loop-level effects (nor considerations from cosmology) which are now harder to dismiss since the behaviour of the model is specified all the way up to the GUT scale.

Maximum rates of ~ 0.3 fb are found for very high values of $\tan\beta$ in a very small region at the corner around the lowest $M_{\frac{1}{2}}$ and M_0 values allowed. The 30 or fewer events expected for 100 fb^{-1} of integrated luminosity would

[11)] It should be noted that the small unexcluded regions shown where the cross section is ~ 0.3–0.01 fb may be partly or totally excluded by the LEP2 Higgstrahlung constraint. However, given the uncertainties surrounding this limit mentioned earlier, we conservatively make no attempt to place exclusion contours from such a process on our plots.

[12)] See [30] for a more complete analysis of the present-day constraints on the mSUGRA parameter space.

probably be unresolvable from amongst the backgrounds. Coincidentally, the signal rate has a minimum at around $\tan\beta = 10$. As $\tan\beta$ drops from 10, the rate briefly rises and then drops again as the production cross section hits its minimum around $\tan\beta = 6$. Above $\tan\beta = 10$, rates again rise, slowly, as $\tan\beta$ grows large (unlike the results seen in the previous section). If $\tan\beta$ is made enormous, then stau inputs must be made very high (while one would like to — but in mSUGRA cannot — keep the other soft slepton inputs low to get a good decay rate) to avoid the LEP2 bound on the physical stau mass.

Given the very meager chances of extracting a signal with the low BRs in the perhaps overly-generous allowed regions of parameter shown here, a more thorough mSUGRA analysis would probably be irrelevant.

4 Detector Simulation Analysis

In the previous sections we outlined the potential for observing the charged Higgs bosons through their decays into charginos and neutralinos, eventually yielding three leptons plus missing energy, and in the presence of a hadronically reconstructed top (anti)quark. As a next step, we study the feasibility of detecting such a signal in a realistic LHC detector environment (CMS). We use the MC event generator HERWIG (version 6.3) and simulate the $gb \to tH^- + \text{c.c.} \to 3\ell + p_T^{\rm miss} + t$ signal for the three MSSM settings already discussed, which we specify more fully here:

- Set A: $M_2 = 210\,\text{GeV}$, $\mu = 135\,\text{GeV}$, $m_{\tilde{\ell}_R} = 110\,\text{GeV}$, $m_{\tilde{g}} = 800\,\text{GeV}$, $m_{\tilde{q}} = 1\,\text{TeV}$.
- Set B: $M_2 = 280\,\text{GeV}$, $\mu = 150\,\text{GeV}$, $m_{\tilde{\ell}_R} = 130\,\text{GeV}$, $m_{\tilde{g}} = 900\,\text{GeV}$, $m_{\tilde{q}} = 1\,\text{TeV}$.
- Set C: $M_2 = 300\,\text{GeV}$, $\mu = -150\,\text{GeV}$, $m_{\tilde{\ell}_R} = 150\,\text{GeV}$, $m_{\tilde{g}} = 1\,\text{TeV}$, $m_{\tilde{q}} = 1\,\text{TeV}$.

Recall that in all settings we assume $M_1 = \frac{5}{3}\tan^2\theta_W M_2$. Furthermore, for sleptons and squarks we will always take soft mass inputs for all generations to be degenerate (with $m_{\tilde{\ell}_L} = m_{\tilde{\ell}_R}$). The physical sneutrino masses, $m_{\tilde{\nu}}$, can be derived from the above parameters and are approximately 90, 115 and 135 GeV for the respective scenarios (when $\tan\beta \gtrsim 5$). Parameter Set A lies inside the optimal region in the three-dimensional (M_2, μ, $m_{\tilde{\ell}_R}$) space identified in Sect. 2, whereas Set B is a more borderline case and Set C is a difficult case with a negative μ parameter. Set A features light inos and sleptons, allowing several supersymmetric $H^\pm$ decay modes to have considerable BRs for relatively moderate values of m_A (and $m_{H^\pm}$). The ino sectors in Set B and Set C are heavier, thereby limiting the number of possible sparticle decay modes. In Set B sleptons are light, whereas in Set C these sparticles are also heavy. This last difference markedly alters the kinematics in ways to be discussed shortly. The MSSM sparticle spectrum and decays are obtained from ISASUSY 7.58 [31] through the ISAWIG interface [32]. ISASUSY contains a one-loop treatment of all Higgs boson masses and tree-level sfermion masses. Several three-body decays are included, taking into account the full Yukawa contributions, which are important in the large $\tan\beta$ regime. The charged Higgs boson BRs are taken from HDECAY [33] (again, via the ISAWIG interface), which calculates these in accordance with the most recent theoretical knowledge. For the SM backgrounds, all leading processes that can produce the $3\ell + p_T^{\rm miss} + t$ signature have been simulated: $t\bar{t}$ ($t\bar{b}W^-$ typically is 1/4 as large), $t\bar{t}Z$, $t\bar{t}\gamma^*$ and $t\bar{t}h$. Furthermore, all SUSY backgrounds have been considered for the chosen settings: ino pair production (including squark+ino production), squark and/or gluino production and slepton pair production. Of these, the first listed class of SUSY contributions has the largest cross sections in general, because inos are fairly light in comparison to the coloured sparticles. In our scenarios, slepton pair production never results in a three lepton final state[13], so that it will be excluded from further consideration. The detector aspects were simulated using CMSJET 4.801 [34], which contains fast parametrisations of the CMS detector response and, for b-tagging, a parametrised track reconstruction performance based on GEANT simulations [35].

In Parameter Set A, the neutralinos $\widetilde{\chi}_1^0$, $\widetilde{\chi}_2^0$, $\widetilde{\chi}_3^0$ and $\widetilde{\chi}_4^0$ have masses of 78, 131, 146 and 253 GeV, respectively. The masses of the charginos $\widetilde{\chi}_1^\pm$ and $\widetilde{\chi}_2^\pm$ are 108 and 252 GeV. The $H^\pm$ are allowed to decay into all kinematically accessible ino pairs, $\widetilde{\chi}_i^\pm\widetilde{\chi}_j^0$, which in turn can decay into three leptons[14] (electrons and/or muons) plus invisible neutral particles ($\widetilde{\chi}_1^0$s and/or neutrinos). In this scenario, the primary source of three-lepton events (before any kinematical cuts are considered) is generally charged Higgs boson decays to $\widetilde{\chi}_1^\pm\widetilde{\chi}_2^0$. This is true for $225\,\text{GeV} \lesssim m_A \lesssim 400\,\text{GeV}$ and[15] $\tan\beta \sim 10$. Charged Higgs boson decays to $\widetilde{\chi}_2^\pm\widetilde{\chi}_2^0$ and $\widetilde{\chi}_1^\pm\widetilde{\chi}_4^0$ are also important sources of 3ℓ events in this region of parameter space, and the contributions from these modes grow to equal or

[13] Unless four leptons are produced rather than the usual two, and then one lepton is subsequently disregarded due to having a p_T value too low to pass our cuts. Rates for such events are negligibly small.

[14] Here $i = 1, 2$ $j = 1, 2, 3, 4$; if $j = 1$, then the three leptons must all come from cascade decays of the chargino.

[15] The upper (lower) m_A value drops by $\sim$20 GeV ($\sim$10 GeV) as $\tan\beta$ goes from 10 to 30 (5).

surpass that from $\widetilde{\chi}_1^\pm\widetilde{\chi}_2^0$ decays for $m_A \gtrsim 400\,\text{GeV}$. $\widetilde{\chi}_2^0$ decays almost exclusively via an intermediate state containing an on-shell charged slepton, while $\widetilde{\chi}_1^\pm$ decays through a intermediate state including an on-shell sneutrino. Here though BRs for stau decays rise as $\tan\beta$ grows (in part due to the fact that, for fixed soft slepton mass inputs, the physical mass of the $\widetilde{\tau}_1^\pm$ decreases swiftly as $\tan\beta$ rises to higher values): for $\tan\beta = 5, 10, 20, 30$, the $\widetilde{\chi}_2^0$ BR to staus is about $0.35, 0.42, 0.61, 0.74$, respectively. Additionally, about $1/3$ of the $\widetilde{\chi}_1^\pm$ decays to sneutrinos are to $\widetilde{\nu}_\tau$, and $\widetilde{\chi}_1^\pm$ decays to $\widetilde{\tau}_1^\pm\nu_\tau$ become accessible at $\tan\beta \simeq 11$ with the BR for this decay growing to 0.24 (0.06) when $\tan\beta$ reaches 30 (20). These ino to stau and $\widetilde{\nu}_\tau$ decays reduce the number of $\widetilde{\chi}_2^0 \to \widetilde{\ell}^\pm\ell^\mp$ and $\widetilde{\chi}_1^\pm \to \widetilde{\nu}_\ell\ell^\pm$ decays, where $\ell = e$ or μ, which lead to virtually all the signal events that survive the necessary cuts[16]. Leptonic tau decays are allowed in the event generation, although daughter leptons from these will mostly be rejected during the analysis stage due to their softness (low p_Ts). Crucial mass differences have values[17] of ($m_{\widetilde{\chi}_2^0} - m_{\widetilde{\ell}^\pm}$, $m_{\widetilde{\chi}_1^\pm} - m_{\widetilde{\nu}_\ell}$, $m_{\widetilde{\ell}^\pm} - m_{\widetilde{\chi}_1^0}$) = (∼10-15 GeV, ∼10-22 GeV, ∼35-45 GeV). In all these cases there is enough phase space for most of the resulting leptons to have sufficiently high transverse momenta.

In order to distinguish between the signal and the backgrounds (both SM and MSSM), we will apply a set of selection criteria that will allow us to obtain a favourable signal-to-background ratio using only physically well-motivated cuts (*i.e.*, with only a very loose dependence upon the MSSM parameters). We will first explain the selection strategy and then illustrate the results numerically in a table.

First of all we require the following basic topology:

- Events must have exactly three isolated leptons ($\ell = e, \mu$) with $p_T > 20, 7, 7\,\text{GeV}$, all with $|\eta| < 2.4$. The isolation cut demands that there are no charged particles with $p_T > 1.5\,\text{GeV}$ in a cone of radius $\Delta R = \sqrt{(\Delta\phi)^2 + (\Delta\eta)^2} = 0.3$ radians around each lepton track and that the sum of the transverse energy deposited in the electromagnetic calorimeter between $\Delta R = 0.05$ and $\Delta R = 0.3$ radians be smaller than $3\,\text{GeV}$.

The choice of the minimum p_T value for the leptons is driven by both trigger and background rejection considerations. In the case of muons, requiring a hardest lepton above $20\,\text{GeV}$ is already sufficient for the event to be triggered with 90% efficiency by the single-muon trigger under low luminosity running conditions at the LHC (for electrons this threshold is somewhat higher) [36]. Apart from the single leptons triggers, the di- and trilepton thresholds will increase the efficiency for triggering on the 3ℓ signal. The tight isolation criterion is needed in order to reject leptons coming from heavy flavour decays, especially in the low p_T region. As we will discuss later, it is very effective against, for instance, the $t\bar{t}$ background, when one or more of the leptons originates from a b-jet.

Apart from requiring the three leptons, it is also necessary to reconstruct the (hadronically decaying) top quark that is produced in association with the $H^\pm$ boson. This is mainly motivated by the need to strongly suppress the $t\bar{t}$ and ino-ino backgrounds. A reconstructed top (antitop) quark is recognised via the following cuts:

- Events must have at least three jets, each with $p_T > 20\,\text{GeV}$ in $|\eta| < 4.5$.
- Among these, the three jets that are most likely to come from a top quark decay are selected by minimising $m_{jjj} - m_t$, where m_{jjj} is the invariant mass of the three-jet system. This invariant mass m_{jjj} must be in the range $m_t \pm 35\,\text{GeV}$.
- Two of these three jets are then further selected by minimising $m_{jj} - M_{W^\pm}$. Their invariant mass, m_{jj}, must be in the range $M_{W^\pm} \pm 15\,\text{GeV}$.
- The third jet (*i.e.*, aside from the two jets in the preceding point) must be b-tagged. For this, we require the jet to contain at least two tracks with a significance of the transverse impact parameter $\sigma(ip) = \frac{ip_{xy}}{\Delta ip_{xy}}$ which is larger than 2.

A strong rejection of $t\bar{t}$ events is obtained after the requirement of a hadronically reconstructed top quark in addition to the three leptons. Assuming that the three jets reconstructing m_t are indeed correctly assigned, this requirement means that the second top should provide two leptons (one from the $W^\pm$ and one from the b) while the

[16] If the soft stau mass inputs are made heavier, rather than degenerate with the other soft slepton mass inputs as is done in this analysis, the unprofitable stau channels could be eliminated and the number of events could as much as double for high values of $\tan\beta$.

[17] These numbers depend moderately on $\tan\beta$. Values given here (and later for Sets B & C) cover the range of interest in this work: $5 \leq \tan\beta \leq 30$. Physical slepton masses are those of the first two generations.

third lepton should come from initial/final state radiation ($b, K, \pi, ...$). In this case, two leptons will be in general soft (< 5 GeV) and non-isolated. Another scenario in which $t\bar{t}$ production can lead to a $3\ell + t$ final state is the one where both top quarks have decayed leptonically, and two radiated jets accidentally reconstruct the $W^{\pm}$ mass and then combine with a b-jet from top decay to mimic a hadronically-decaying top quark. Here, two leptons can be hard, but the third one must still be soft and in general non-isolated. Therefore, in order to achieve a sufficient suppression of the $t\bar{t}$ background, we have chosen to set the lower limit on the p_T of the leptons at 7 GeV (although lowering it would increase the signal yield) and to apply a tight isolation criterion.

Whereas the $t\bar{t}$ background is greatly suppressed by the previous selection steps, $t\bar{t}Z$, $t\bar{t}\gamma^*$ and $t\bar{t}h$ events would still survive the $3\ell + t$ criteria. Therefore we require an additional Z-veto:

- Reject all events with di-lepton pairs with opposite charges and the same flavour that have an invariant mass in the range $M_Z \pm 10$ GeV.

The Z-veto rejects $t\bar{t}Z$ events efficiently. Moreover, although the $t\bar{t}\gamma^*$ and $t\bar{t}h$ backgrounds largely survive this requirement, their residual cross sections are now innocuously small.

In addition to eliminating the SM noise, cuts to efficiently suppress the SUSY backgrounds that can lead to a $3\ell + t$ final state must be considered. As mentioned before, slepton pair production does not pose a problem in our scenarios since it cannot lead to a three-lepton final state. Ino pair production and squark+ino production can have large cross sections; however, most events from these processes do not contain a top quark and will thus be rejected via the hadronic top requirement. Events that are still left after this cut form the main irreducible SUSY background. Squark/gluino production is another potentially dangerous source of noise. These events, however, typically contain many energetic jets besides those coming from the top decay (as previously intimated). Therefore, they can be rejected using an additional jet veto:

- Reject all events containing any jets (other than the three jets selected for the top reconstruction) with $p_T > 70$ GeV and $|\eta| < 4.5$.

For further signal-to-background rejection, we impose the following (slightly model dependent) selection criteria (here optimised for $m_A = 350$ GeV and $\tan\beta = 10$):

- For the three isolated leptons already selected, the p_T of the hardest lepton should be below 150 GeV whereas the p_T of the softest lepton should be below 40 GeV.
- The missing transverse energy should be larger than 40 GeV.
- The effective mass, $M_{\rm eff}$, constructed from the $p_T^{3\ell}$ and p_T^{miss} vectors as $M_{\rm eff} = \sqrt{2p_T^{3\ell}p_T^{\rm miss}(1-\cos\Delta\phi)}$, is required to be lower than 150 GeV (here $\Delta\phi$ is the azimuthal angle between $p_T^{3\ell}$ and p_T^{miss}).

The missing energy requirement has little affect on the signal yield since the two $\widetilde{\chi}_1^0$ in the final state usually supply sufficient p_T^{miss}; on the other hand, this cut does reduce the SM $t\bar{t}V$ (V=Z,γ^*) backgrounds. As was shown in [2], the effective mass variable does have some dependence on the ino mass spectrum; but it also proves to be effective against the above $t\bar{t}V$ processes plus squark/gluino and ino pair production backgrounds as well.

After applying these selection criteria, we obtain the number of signal (S) and background (B) events given in Tab. 1, assuming Parameter Set A, with $m_A = 350$ GeV and $\tan\beta = 10$, and for an integrated luminosity of 100 fb^{-1}. Results shown therein clearly confirm the points made in the preceding description of the cuts.

Fig. 7 shows the three-lepton invariant mass distribution for our typical signal ($m_A = 350$ GeV and $\tan\beta = 10$) on top of the background (SM + SUSY) for an integrated luminosity of 100 fb^{-1}. The peak in the three-lepton invariant mass distribution depends both on $m_{H^\pm}$ *and* on the mass spectrum of the intermediate charginos and neutralinos. Therefore, a direct 'parameter-independent' mass reconstruction does not seem feasible at this stage. The determination of the charged Higgs mass will require comparisons between the measured three-lepton invariant mass and MC distributions.

Maintaining the MSSM setup of Parameter Set A, we can now perform a scan over m_A and $\tan\beta$ in order to determine the discovery potential for the '$3\ell + p_T^{\rm miss} + t$' signature we have been considering. We assume an integrated luminosity of 100 fb^{-1} and require the significance of the signal, $S/\sqrt{B}$, to be larger than 5. The resulting 5σ-discovery potential is shown in the top plot of Fig. 8. The left edge of the potential discovery region at $m_A \approx 250$ GeV is determined by the kinematic requirement that $m_{H^\pm} > m_{\widetilde{\chi}_2^0} + m_{\widetilde{\chi}_1^\pm}$. The upper edge in

Process	3ℓ events	Z-veto	hadr. top[†]	b-tag	jet veto[††]	others[†††]
$t\bar{t}$	2781	2465	91	15.5	11.1	5.8
$t\bar{t}Z$	492	82	19	8	2.4	0.8
$t\bar{t}\gamma^*$	22	21	7	2	0.4	0.2
$t\bar{t}h$	59	52	17	4	1.6	0.2
$\widetilde{\chi}\widetilde{\chi}$	19993	18880	237	31	9	3
$\tilde{q}$, $\tilde{g}$	12712	11269	3984	861	6	1
tH^- & $\bar{t}H^+$	508	485	126	36	29	25

Table 1: Number of signal and background events assuming Parameter Set A, with $m_A = 350\,\text{GeV}$ and $\tan\beta = 10$, for $100\,\text{fb}^{-1}$. (Note that the difference between event rates in the 'hadr. top' and the 'b-tag' columns is not only due to the experimental b-tagging efficiency but also takes into account part of the algorithmic efficiency.)
[†]Here, top reconstruction requires ≥ 3 jets with $p_T > 20\,\text{GeV}$, $m_{jj} \sim M_{W^\pm}$ and $m_{jjj} \sim m_t$.
[††]Here, one vetoes additional jets beyond 3 with $p_T > 70\,\text{GeV}$.
[†††]Here, one imposes $p_T(\ell_1) < 150\,\text{GeV}$, $p_T(\ell_3) < 40\,\text{GeV}$, $p_T^{\text{miss}} > 40\,\text{GeV}$ and $M_{\text{eff}} < 150\,\text{GeV}$.

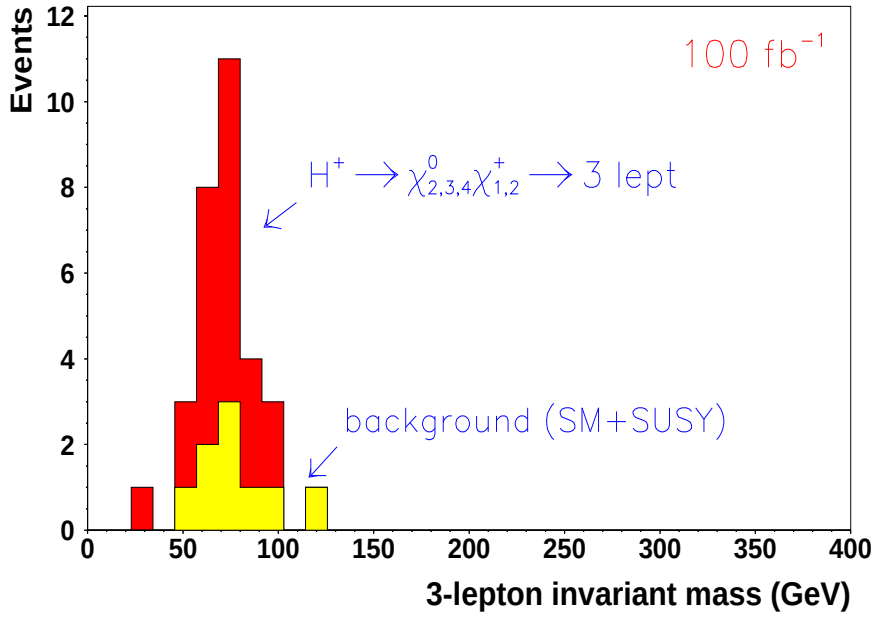

Figure 7: Three-lepton invariant mass distribution for Parameter Set A, with $m_A = 350\,\text{GeV}$ and $\tan\beta = 10$. The signal peak is shown on top of the SM + SUSY background for an integrated luminosity of $100\,\text{fb}^{-1}$, after all cuts described in the text.

$\tan\beta$ originates from decreasing $H^\pm \to \widetilde{\chi}_i^\pm \widetilde{\chi}_j^0$ and $\widetilde{\chi}_j^0 \to \ell^+\ell^-\widetilde{\chi}_1^0$ ($i = 1, 2$ and $j = 2, 3, 4$) BRs. This is in part a consequence of the high $\tan\beta$ enhancement of $H^\pm$ couplings to the third generation (taus, top and bottom quarks), which grow at the expense of the couplings to the inos (the intermediates we need to get our hard, isolated electrons and muons) and in part due to the increased BRs for ino decays into staus, which grow at the expense of decays into lepton(e and μ)-yielding selectrons and smuons. The upper edge in m_A and lower edge in $\tan\beta$ are determined by the m_A and $\tan\beta$ dependence of the production cross section. Conservative LEP exclusion limits [37], mainly from Higgstrahlung (*i.e.*, $e^+e^- \to hZ$ and $e^+e^- \to hA$), are also drawn in the figure along with a horizontal dotted line below which $m_{\widetilde{\chi}_1^\pm}$ does not respect the LEP2 bound[18)].

[18)] Not shown on the plots in Fig. 8 are upper $\tan\beta$ bounds of 32.2, 28.9, and 44.0 for Parameter Sets A, B and C, respectively, above which the lighter stau mass dips below the LSP ($\widetilde{\chi}_1^0$) mass. This bound may be evaded by raising the soft stau mass inputs above those of the first two generations of sleptons.

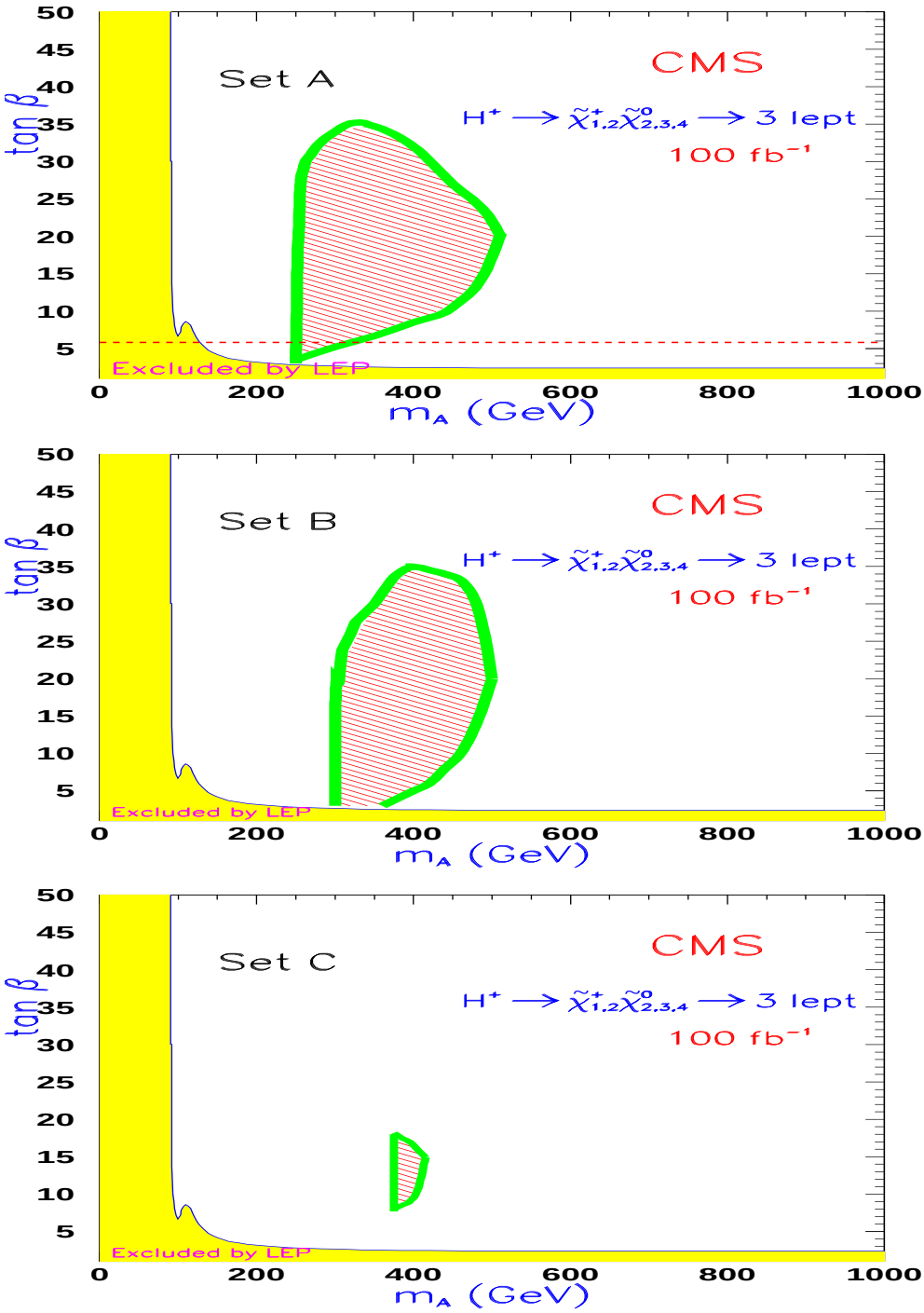

Figure 8: 5σ-discovery contours in the $\tan\beta$ *vs.* m_A plane for Parameter Sets A, B and C, assuming an integrated luminosity of $100\,\text{fb}^{-1}$. The shaded region at the left and bottom of each plot is excluded by LEP2 Higgstrahlung (*i.e.*, $e^+e^- \to hZ$ and $e^+e^- \to hA$) limits. The region in the top plot below the red dotted line is excluded by the LEP2 chargino mass bound.

Parameter Set B produces the following mass spectrum: the neutralinos $\widetilde{\chi}_1^0$, $\widetilde{\chi}_2^0$, $\widetilde{\chi}_3^0$ and $\widetilde{\chi}_4^0$ have masses of 103, 159, 165 and 311 GeV, respectively, while the masses of the charginos $\widetilde{\chi}_1^\pm$ and $\widetilde{\chi}_2^\pm$ are 131 and 311 GeV. The 5σ-discovery potential for this setting, again for an integrated luminosity of $100\,\text{fb}^{-1}$, is presented in the middle plot of Fig. 8, after the usual selection procedure. A noticeable difference with respect to Parameter Set A is that here the discovery zone starts at somewhat higher values of m_A due to the higher $m_{H^\pm}$ threshold needed for

decays to ino pairs, since they are heavier than in the previous scenario. For $m_A \gtrsim 300$ GeV, $H^\pm \to \widetilde{\chi}_1^\pm \widetilde{\chi}_3^0$ is the dominant source of 3ℓ events, rather than $H^\pm \to \widetilde{\chi}_1^\pm \widetilde{\chi}_2^0$ as in the previous scenario[19]. There are two reasons for this change: firstly, with Set B, $\widetilde{\chi}_3^0$ has a more favourable gaugino/Higgsino mixing than does $\widetilde{\chi}_2^0$; and secondly, for Set B BRs for $\widetilde{\chi}_2^0$ decays into sneutrino spoiler modes for $\tan\beta = 5, 10, 20, 30$ are about 85%,84%,68%,39%, whereas for Set A these values are all roughly 0.5%. $H^\pm \to \widetilde{\chi}_1^\pm \widetilde{\chi}_3^0$ decays remain the dominant source of 3ℓ events even for high charged Higgs boson masses. The $H^\pm \to \widetilde{\chi}_2^\pm \widetilde{\chi}_2^0$ and $H^\pm \to \widetilde{\chi}_1^\pm \widetilde{\chi}_4^0$ decay modes, which led to the majority of the three lepton events for a ∼450 GeV charged Higgs boson with Set A, in Set B are no longer dominant for higher $m_{H^\pm}$ values, at most providing ∼30% of the events (before cuts) for $m_{H^\pm} \sim 650$ GeV (for which mass value the production rate is already too low for any hope of discovery). The $\widetilde{\chi}_3^0$ decays predominantly into a charged slepton; the BR for $\widetilde{\chi}_3^0$ decays into staus grows from ∼32.5% to ∼47.5% as $\tan\beta$ goes from 5 to 30, cutting into the desired decays to selectrons and smuons. Though $\widetilde{\chi}_3^0$ decay modes to sneutrinos are accessible too, the combined BR for such spoiler modes remain at the 3-4% level. The $\widetilde{\chi}_1^\pm$ decays through a sneutrino intermediate state and the associated charged lepton[20]. Crucial mass differences have values of ($m_{\widetilde{\chi}_3^0} - m_{\widetilde{\ell}^\pm}$, $m_{\widetilde{\chi}_1^\pm} - m_{\widetilde{\nu}_\ell}$, $m_{\widetilde{\ell}^\pm} - m_{\widetilde{\chi}_1^0}$) = (∼25-30 GeV, ∼12-22 GeV, ∼30-40 GeV). As in Set A, there is enough kinematical phase space for most of the resulting leptons to have sufficiently high transverse momenta to pass the signal selection criteria.

In Parameter Set C the neutralinos $\widetilde{\chi}_1^0$, $\widetilde{\chi}_2^0$, $\widetilde{\chi}_3^0$ and $\widetilde{\chi}_4^0$ have masses of 118, 162, 171 and 324 GeV, respectively. The masses of the charginos $\widetilde{\chi}_1^\pm$ and $\widetilde{\chi}_2^\pm$ are 143 and 324 GeV. Scanning over m_A and $\tan\beta$, after the customary selection cuts, now leads to the 5σ-discovery potential seen in the bottom plot of Fig. 8. The reach both in m_A and $\tan\beta$ is strongly reduced in comparison to the previous scenarios, in part due to the heavier ino mass spectrum which gives the expected upwards shift of the left edge in m_A. As with Set B, $H^\pm \to \widetilde{\chi}_1^\pm \widetilde{\chi}_3^0$ is the dominant source of signal events for $m_A \lesssim 600$ GeV ($m_A \lesssim 520$ GeV) and $\tan\beta \simeq 5$ (30). For 350 GeV $< m_A <$ 450 GeV, virtually all (> 90%) signal events come via this channel. For higher masses, $H^\pm \to \widetilde{\chi}_1^\pm \widetilde{\chi}_4^0$ and $H^\pm \to \widetilde{\chi}_2^\pm \widetilde{\chi}_3^0$ contributions grow to become comparable. Also, as with Set B, the $\widetilde{\chi}_3^0$ decays predominantly into a charged slepton; again decays into staus — BR ∼29% (∼58%) for $\tan\beta = 5$ (30) — cut into the desired decays to selectrons and smuons. The sneutrino spoiler modes also have a combined BR roughly in the 10-20% range. The $\widetilde{\chi}_1^\pm$ decays through a sneutrino intermediate state: for $\tan\beta < 20$, about $2/3$ of the time into sneutrinos of the first two generations and about $1/3$ of the time into a $\widetilde{\nu}_\tau$ and the associated τ-lepton. For higher values of $\tan\beta$, the $\widetilde{\chi}_1^\pm \to \widetilde{\tau}_1^\pm \nu_\tau$ decay mode becomes accesssible and reaches a BR of almost 70% by the time $\tan\beta$ reaches 30. Now crucial mass differences have values of ($m_{\widetilde{\chi}_3^0} - m_{\widetilde{\ell}^\pm}$, $m_{\widetilde{\chi}_1^\pm} - m_{\widetilde{\nu}_\ell}$, $m_{\widetilde{\ell}^\pm} - m_{\widetilde{\chi}_1^0}$) = (∼13-17 GeV, ∼4-10 GeV, ∼30-45 GeV). Most significantly, there is considerably less phase space available to leptons produced in chargino to sneutrino decays[21]; thus, said leptons are typically too soft and usually fail the p_T cut. This explains the much smaller discovery reach for Set C compared to the one for Set B.

For $\mu < 0$, the same magnitude of $|\mu|$ leads to heavier inos (in particular, the LSP and lighter chargino). Thus, for a fixed $|\mu|$, we expect a smaller signal rate for $\mu < 0$ than for $\mu > 0$. However, the more rapid rise of the chargino mass as $|\mu|$ increases with $\mu < 0$ also means that we can go to smaller $|\mu|$ values on this side before we run afoul of the LEP2 excluded region[22]. Thus, one can shift to lower $|\mu|$ values on the $\mu < 0$ side to obtain roughly the same rates as found on the $\mu > 0$ side (*cf.*, Fig. 4 of [2]).

Some perspective as to the new regions of MSSM parameter space that might be probed via the '$3\ell + p_T^{\rm miss} + t$' channel is provided by Fig. 9, which shows the reach of this $H^\pm \to$ inos signature in the case[23] of Parameter Set A together with those of the $H^- \to \tau^- \bar{\nu}_\tau$ and $H^- \to b\bar{t}$ channels, with $\tan\beta$ plotted on a logarithmic scale to better illustrate the intermediate $\tan\beta$ regime. The discovery reaches for channels where the $H^\pm$ decays to SM particles also assume Set A MSSM input parameters and LO normalisation for the production process; however,

[19] For Set B, there is a thin strip of parameter space around $m_A \sim$ 280-290 GeV in which $H^\pm \to \widetilde{\chi}_1^\pm \widetilde{\chi}_2^0$ is the dominant source of 3ℓ events. However, the overall 3ℓ BR drops precipitously in this region as m_A decreases, and so there is no potential for discovery.

[20] Chargino decays to $\widetilde{\tau}_1^\pm \nu_\tau$ become significant for higher values of $\tan\beta$: this BR is ∼21% (∼6%) for $\tan\beta = 30$ (20). Not so useful decays to $\widetilde{\nu}_\tau \tau^\pm$ have BRs of 34-37%.

[21] The difference between $m_{\widetilde{\chi}_1^\pm} - m_{\widetilde{\nu}_\ell}$ for Set C and the values for Sets A & B is more striking when $\tan\beta$ is restricted to be ≥ 10. Then for A and B $m_{\widetilde{\chi}_1^\pm} - m_{\widetilde{\nu}_\ell}$ ∼17-22 GeV while for C the value is ∼4-7 GeV, with this mass difference growing with increasing $\tan\beta$ for A and B and shrinking with increasing $\tan\beta$ for C.

[22] This is traceable to a term $\propto 2\mu M_2 \sin 2\beta$ in the formula for the chargino mass, and hence the asymmetry diminishes as the $\tan\beta$ value increases.

[23] The authors caution that this figure is valid for a specific set of the MSSM inputs M_2, μ and $m_{\tilde{\ell}_R}$, not in general.

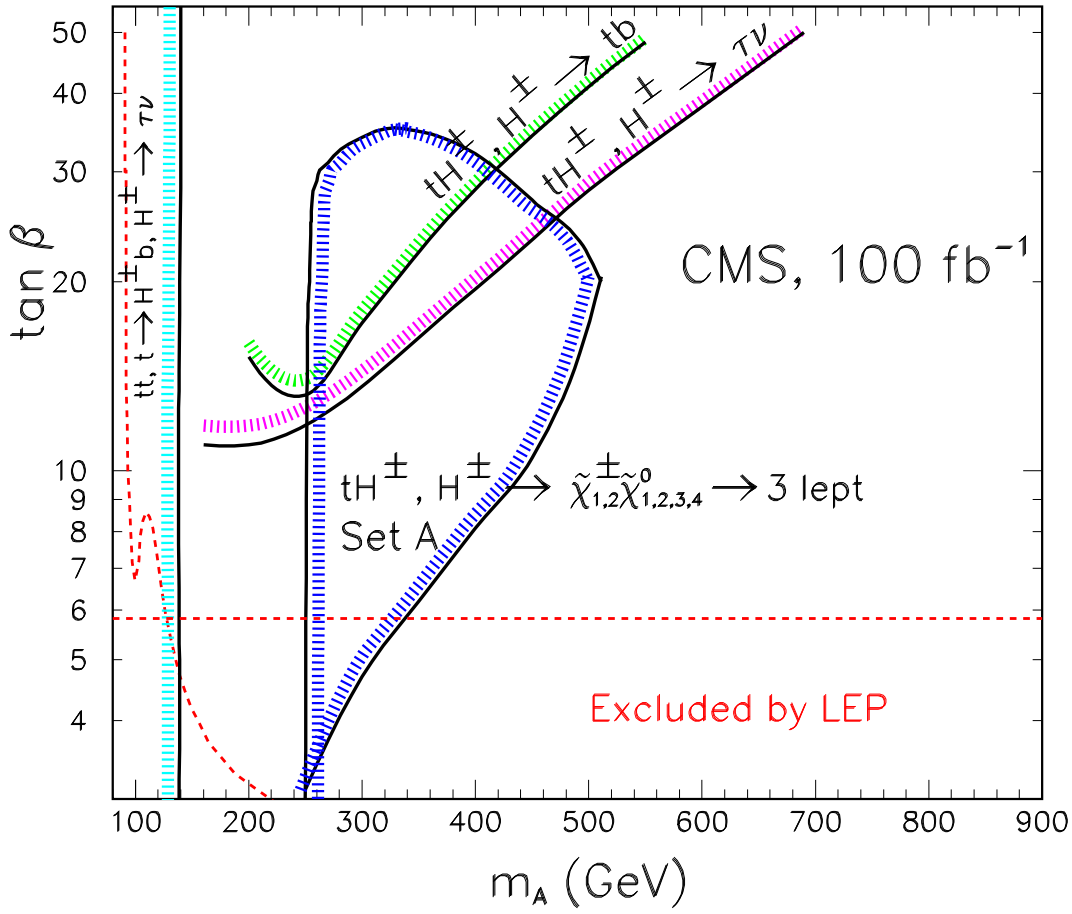

Figure 9: 5σ-discovery contours in the $\tan\beta$ *vs.* m_A plane for all charged Higgs channels, both SM and MSSM, assuming MSSM inputs as in Parameter Set A and 100 fb^{-1} of integrated luminosity. The area below the red dotted line at the left is excluded by LEP2 Higgstrahlung (*i.e.*, $e^+e^- \to hZ$ and $e^+e^- \to hA$) limits and the region below the horizontal red dotted line is excluded by the LEP2 chargino mass bound.

said contours do not take into account possible SUSY backgrounds. The contour for $H^- \to b\bar{t}$ also only takes into account the $3b$-final state analysis [38]. More detailed studies, including $4b$-final states, are ongoing. However, we do not expect major changes in the $(m_A, \tan\beta)$ reach for this channel. Similar plots combining the SM and MSSM channels can be drawn for the other two MSSM parameter sets. Comparison of the "tb" and "$\tau\nu$" contours in Fig. 9 with the analogous discovery regions in [4], which used $\mu = -200\,\text{GeV}$ and $M_2 = 200\,\text{GeV}$ as inputs, show the former contours to have shrunk somewhat relative to the latter ones, as expected since the combined BR($H^\pm \to$ inos) is larger in relevant parts of the $(m_A, \tan\beta)$ plane for Set A inputs than for the inputs of [4]. This shows that the ino decays will reduce the rates for the conventional $H^\pm$ signatures. In particular, relative to a case where the ino decay modes are closed (such as when $|\mu|$, M_2, and sfermion masses are all large) the SM-like discovery regions may be significantly reduced. This makes the search for the '$3\ell + p_T^{\text{miss}} + t$' signature from $H^\pm \to$ inos decays all the more important.

5 Conclusions

In summary, we have proven that SUSY decays of charged Higgs bosons can profitably be exploited at the LHC in order to detect these important particles. We have done an extensive probe of the MSSM parameter space to see where decays of the type $H^\pm \to \widetilde{\chi}_i^\pm \widetilde{\chi}_j^0$, $(i = 1, 2,\ j = 1, 2, 3, 4)$ can yield hadronically quiet three lepton (electrons and/or muons) final states. Here all tree-level decay chains allowable within the MSSM have been taken into account. Coupling such decay chains with top-associated charged Higgs boson production, we selected a signature consisting of three hard isolated leptons (electrons and/or muons), three hard jets which reconstruct the top quark (with one pair thereof also reconstructing a $W^\pm$ boson and the other bearing a b-tag) and substantial missing transverse energy. We then performed quite realistic MC studies utilising the HERWIG event generator

and modelling the CMS detector. The hard subprocess used for the signal was $gb \to tH^-$ (and c.c.), supplemented by initial and final state parton shower and hadronisation, with overall LO normalisation. (All backgrounds were generated at the same level of accuracy.) Recent studies [23] have found that there are substantial positive NLO corrections to said LO signal rates, yielding an enhancement K-factor of $\gtrsim 1.6$, comparable to or even larger than the corresponding corrections for the leading backgrounds. Inclusion of such NLO effects in future signal and background analyses may well expand the discovery reach of this channel.

We found that this '$3\ell + p_T^{\rm miss} + t$' signature has the potential to provide coverage over an area of the MSSM parameter space roughly corresponding to $250\,{\rm GeV} < m_{H^\pm} < 500\,{\rm GeV}$ and $3 \lesssim \tan\beta \lesssim 35$. This region covers a substantial portion of parameter space where $H^\pm$ decays into ordinary particles have been shown to be ineffective. However, to this must be added the *caveat* that other MSSM input parameters must be favourable. To wit, a small value for $|\mu|$ and a small to moderate M_2 value are essential for having substantial $H^\pm \to \widetilde{\chi}_i^\pm \widetilde{\chi}_j^0$ BRs (with $M_2 > |\mu|$ to put more weight on ino decays not including the LSP) and light sleptons are crucial for enhancing the leptonic BRs of the inos. Said slepton intermediates may be on- or off- mass shell; though of course it is optimal if the two-body on-shell ino decay mode into a slepton and a lepton is open, as shown by Fig. 5. Naturally, the actual physical masses of the sleptons (selectrons, smuons and the associated sneutrinos) should be less than those of an ino pair into which the charged Higgs boson has a significant BR. Depending on the ino masses as fixed by the MSSM parameter inputs, this dictates slepton masses of $\lesssim 160\,{\rm GeV}$ or lower in the discovery regions documented in this work.

Regions in MSSM parameter space satisfying such criteria tend to be sufficiently close to the LEP2 limits and/or to those derived after Run 2 at the Tevatron that such regions should be readily accessible to probing by the LHC. We have made very few assumptions about the underlying SUSY-breaking dynamics associated with some much higher energy scale, and hence defined all relevant MSSM input parameters at the EW scale. (The mSUGRA model was analysed as a possible GUT benchmark but failed to shown any potential for the considered decay channel.) The discovery reach shown in Fig. 9 (for a reasonably favourable choice of these parameters) illustrates the possible power of this new channel.

Acknowledgments

MB is grateful to the U.S. National Science Foundation for support under grant INT-9804704. FM is a Research Assistant of the Fund for Scientific Research - Flanders (Belgium). The authors would like to thank the IUAP/PAI network "Fundamental Interactions" funded by the Belgian Federal Government. FM would like to thank Daniel Denegri and Luc Pape for discussions.

References

[1] J.F. Gunion, H.E. Haber, G.L. Kane and S. Dawson, "The Higgs Hunter Guide" (Addison-Wesley, Reading MA, 1990), *Erratum*, `hep-ph/9302272`.

[2] M. Bisset, M. Guchait and S. Moretti, Eur. Phys. J. C 19, 143 (2001).

[3] K.A. Assamagan *et al.*, `hep-ph/0203056`; S. Moretti, `hep-ph/0205104`.

[4] See, *e.g.*: D. Denegri *et al.*, `hep-ph/0112045`.

[5] F. Moortgat, S. Abdullin and D. Denegri, `hep-ph/0112046`.

[6] K.A. Assamagan and Y. Coadou, ATL–COM–PHYS–2000–017; K.A. Assamagan , Y. Coadou and A. Deandrea, Eur. Phys. J. direct C9, 1 (2002).

[7] H. Baer, M. Bisset, D. Dicus, C. Kao and X. Tata, Phys. Rev. D 47, 1062 (1993); H. Baer, M. Bisset, C. Kao and X. Tata Phys. Rev. D 50, 316 (1994); M. Bisset, Univ. of Hawaii at Manoa Ph.D. Dissertation, UH-511-813-94 (1994).

[8] H. Baer, D.A. Dicus, M. Drees and X. Tata, Phys. Rev. D 36, 1363 (1987); J.F. Gunion *et al.*, Int. J. Mod. Phys. 2, 1035 (1987); K. Griest and H.E. Haber, Phys. Rev. D 37, 719 (1988); A. Djouadi, J. Kalinowski and P.M. Zerwas, Z. Phys. C 57, 569 (1993); A. Djouadi, J. Kalinowski, P. Ohmann and P.M. Zerwas, Z. Phys. C 74, 93 (1997).

[9] J.F. Gunion and H.E. Haber, Nucl. Phys. B 307, 445 (1988), *ibid.* B 278, 449 (1986), *ibid.* B 272, 1 (1986), *Erratum*, *ibid.* B 402, 567 (1993).

[10] See: LEP Higgs Working Group web page, `http://lephiggs.web.cern.ch/LEPHIGGS/papers/`.

[11] M. Carena, J.S. Conway, H.E. Haber and J.D. Hobbs (conveners), proceedings of the 'Tevatron Run II SUSY/Higgs' Workshop, Fermilab, Batavia, Illinois, USA, February-November 1998, `hep-ph/0010338`.

[12] D. Chakraborty, in Ref. [11]; M. Guchait and S. Moretti, J. High Energy Phys. 01, 001 (2002).

[13] M. Misiak, S. Pokorski, and J. Rosiek, `hep-ph/9703442`; P.H. Chankowski and S. Pokorski, `hep-ph/9707497`; J. Erler and D.M. Pierce, Nucl. Phys. B 526, 53 (1998).

[14] C. Degrassi, P. Gambino and G.F. Giudice, J. High Energy Phys. 12, 009 (2000); M. Carena, D. Garcia, U. Nierste and C.E.M. Wagner, Phys. Lett. B 499, 141 (2001); A.J. Buras, P.H. Chankowski, J. Rosiek and Ł. Sławianwska, `hep-ph/0210145`; K.-I. Okumura and L. Roszkowski, `hep-ph/0208101`. See Ref. [13] of [2] for a cross section of MSSM $b \to s\gamma$ literature; for a discussion of the current status of $b \to s\gamma$ calculations, see P. Gambino, J. Phys G 27, 1199 (2001).

[15] G. Isidori, Phys. Lett. B 298, 409 (1993); Y. Grossman, H.E. Haber, and Y. Nir, Phys. Lett. B 357, 630 (1995).

[16] S.P. Martin and J.D. Wells, Phys. Rev. D 64, 035003 (2001); M. Byrne, C. Kolda and J.E. Lennon, `hep-ph/0208067`.

[17] A.F. Falk, Nucl. Instrum. Meth. A 408, 7 (1998); A.L. Kagan and M Neubert, Eur. Phys. J. C 7, 5 (1999).

[18] A. Brignole, J. Ellis, G. Ridolfi and F. Zwirner, Phys. Lett. B 271, 123 (1991); A. Brignole, Phys. Lett. B 277, 313 (1992); M.A. Díaz and H.E. Haber, Phys. Rev. D 45, 4246 (1992).

[19] H. Baer and X. Tata, Phys. Rev. D 47, 2739 (1993).

[20] See: LEP SUSY Working Group web page, `http://www.cern.ch/LEPSUSY/`.

[21] F. Borzumati, J.-L. Kneur and N. Polonsky, Phys. Rev. D 60, 115011 (1999); S. Moretti and D.P. Roy, Phys. Lett. B 470, 209 (1999).

[22] A. Belyaev, D. Garcia, J. Guasch and J. Solà, Phys. Rev. D 65, 031701 (2002), J. High Energy Phys. 06, 059 (2002).

[23] S.-H. Zhu, `hep-ph/0112109`; T. Plehn, `hep-ph/0206121`.

[24] S. Moretti *et al.*, J. High Energy Phys. 04, 028 (2002); S. Moretti, `hep-ph/0205105`.

[25] G. Corcella *et al.*, `hep-ph/9912396`, J. High Energy Phys. 01, 010 (2001), `hep-ph/0107071`, `hep-ph/0201201`, `hep-ph/0210213`.

[26] W. Beenakker, R. Hopker and M. Spira, `hep-ph/9611232`.

[27] T. Affolder *et al.* (CDF Collaboration), Phys. Rev. Lett. 88, 041801 (2002); D.E. Groom *et al.* (Particle Data Group), Eur. Phys. J. C 15, 1 (2000).

[28] L. Alvarez Gaumé, J. Polchinski and M. Wise, Nucl. Phys. B 221, 495 (1983); J.-M. Frère, D.R.T. Jones and S. Raby, Nucl. Phys. B 222, 11 (1983); M. Claudson, L. Hall and I. Hinchliffe, Nucl. Phys. B 228, 501 (1983); H.P. Nilles, M. Srednicki and D. Wyler, Phys. Lett. B 120, 346 (1983); H. Baer, M. Brhlik and D. Castano, Phys. Rev. D 54, 6944 (1996); J.A. Casas, A. Lleyda and C. Muñoz, Nucl. Phys. B 471, 3 (1996), Phys. Lett. B 380, 59 (1996), *ibid.* B 389, 305 (1996); S.A. Abel and C.A. Savoy, Nucl. Phys. B 532, 3 (1998), Phys. Lett. B 444, 119 (1998).

[29] M. Bisset, S. Moretti and F. Moortgat, in preparation.

[30] M. Battaglia *et al.*, Eur. Phys. J. C 22, 535 (2001); A. Djouadi, M. Drees and J.L. Kneur, J. High Energy Phys. 0108, 055 (2001); U. Chattopadhyay and P. Nath, Phys. Rev. D 66, 093001 (2002); W. de Boer, M. Huber, C. Sander and D.I. Kazakov, `hep-ph/0106311`.

[31] H. Baer, F.E. Paige, S.D. Protopopescu and X. Tata, hep-ph/0001086.

[32] See:
http://www-thphys.physics.ox.ac.uk/users/PeterRichardson/HERWIG/isawig.html.

[33] A. Djouadi, J. Kalinowski and M. Spira, Comput. Phys. Commun. 108, 56 (1998).

[34] S. Abdullin, A. Khanov and N. Stepanov, CMS NOTE-1994/180.

[35] The CMS Simulation Package:
http://cmsdoc.cern.ch/cmsim/cmsim.html.

[36] CMS Collaboration, "The Trigger and DAQ Paroject, Vol. 2, The High Level Trigger, Technical Design Report", CERN/LHCC 2002-026, CMS TDR 6.2, December 2002.

[37] The LEP Higgs working group, hep-ex/0107030.

[38] P. Salmi, R. Kinnunen and N. Stepanov, CMS NOTE-2002/024;
R. Kinnunen, private communication.